A NOVEL PHYSICAL INVESTIGATION OF SALT INTERACTIONS WITH LIPID MEMBRANES

Supervisor: Rob Barker

Chemistry Research Masters Thesis

Charlotte Byford
ceb69@kent.ac.uk

Contents

1) Acronyms

- PS – Phosphatidylserine
- LBLENP's – Lipid bilayer encapsulated nanoparticles
- SLB – Supported lipid bilayers
- POPC – 1,2 – palmitoyl-oleoyl-sn-glycerol-3-phosphocholine
- FCS – Fluorescence correlation spectroscopy
- MD – Molecular dynamic
- DMPC – 1,2-Dimyristoyl-sn-glycero-3-phosphocholine
- DPPC – Dipalmitoylphosphatidylcholine
- DSPC – Distearoylphosphatidylcholine
- PC – Phosphatidylcholine
- DDA – Dielectric Dispersion Analysis
- DLPE - 1,2-Dilauroyl-sn-glycero-3-phosphoethanolamine
- PE – Phosphatidylethanolamine
- ATP – Adenosine Triphosphate
- DMPS – Di-myristoyl-phosphatidyl-serine
- DMPG - 1,2-Dimyristoyl-sn-glycero-3-phosphoglycerol
- DPPS - 1,2-Dipalmitoyl-sn-glycero-3-phosphoserine
- DPPG - 1,2-Dipalmitoyl-sn-glycero-3-phosphoglycerol
- POPG - 1-palmitoyl-2-oleoyl-sn-glycero-3-phosphoglycerol
- ATR – FTIR - Attenuated total reflectance Fourier transform infrared spectroscopy
- ATM – Atomic Force Microscopy
- HEPES – (4 – (2 – hydroxyethyl)-1-piperazine-ethanesulfonic acid)
- RCA - Radio Corporation of America
- UPW – Ultra Pure Water
- PTFE – Polytetrafluoroethylene
- RMS – Root Mean Square
- SLD -Scattering Length Density
- hDPPC – hydrogenated 1,2-dipalmitoyl-sn-glycero-3-phosphocholine

2) Abstract

The transport of molecules and compounds across cell membranes is vital for life and a process that has been the topic of intricate research for some time. However, it has been a challenge due to cell membranes dynamic and complex nature. It has been known for years that an effective way to undergo this research was to investigate the interactions of lipid membranes, these serve as an appropriate mimic to the cell membranes, and by looking at molecule – lipid interactions it can greatly help to predict the mechanisms of transport and furthermore the effects of these interactions.

The following work explores the area of salt interactions with lipid membranes. It is well known that various salts have significant importance on bodily functions and physiological impacts yet their interactions with membranes seem obscure. In order to attempt to elucidate this topic of research, an investigation was carried out which focuses on sodium and calcium interactions with monolayers and bilayers. This was conducted using a Quartz Crystal Microbalance, Langmuir-Schaefer deposition and data retrieved Neutron reflectometry experiments. Whereby the aim of these experiments was to provide a coherent and thorough practical study to be considered along the vast simulation studies present in this area of research.

The QCM data revealed some lipid loss overall. Although some of this may have been due to the initial lipid deposition as there is evidence suggesting some aggregates forming. This loss of lipid occurred more erratically for NaCl than it did for $CaCl_2$. Unfortunately, due to faults in the QCM system and software, data from higher concentrations of $CaCl_2$ was unable to be retrieved, therefore a full comparison could not be made between sodium and calcium QCM runs. For the Langmuir isotherms which focused on monolayers, an overall decrease in area per molecule was observed. Similar to the QCM, this implied disruption of the lipid. Although a more in-depth look into the data also suggests a possibility of monolayer saturation. The data also provides an indication towards Ion bridging occurring between lipids, however this only seen with the $CaCl_2$ isotherm.

Neutron reflectometry data was collected from a single bilayer of hDPPC in an $CaCl_2$ subphase, this data was then fit with Rascal software. The SLD profiles revealed that the salt solutions applied had little effect on the bilayer and the interaction was minimal. When comparing the neutron data to the QCM or Langmuir it was proven difficult as any loss of lipid as implied prior would have been beyond the detection of a neutron reflectometry experiment due to the resolution being too high. Neutron reflectometry data was also collected from SURF on floating bilayers, this was also fit using Rascal. Again, the floating bilayer experienced little change with the addition of $CaCl_2$ overall. However, a more in-depth look was conducted investigating the fluid and gel phases. It was here that the results revealed affects to the parameter values which further implied ion bridging and the lipid disruption much like the Langmuir isotherm data.

An overview of the results revealed a concurrence that the addition of NaCl and $CaCl_2$ salt solutions to DPPC lipid membranes had little effect, however it is shown that the methods provided evidence leading to suggested disruptions in the lipid, the QCM demonstrated this through mass losses, whilst the isotherms and neutron reflectometry experiments displayed overlaps in data. Therefore, it can be confidently said that the experiments met the aims of the study, which was to provide practical evidence of salt interactions with lipid membranes. This is promising for future work as shows potential for practical avenues to be explored in this topic that can be combined with simulation studies.

3) Introduction

a) Salts in Biology/Biophysics:

The study of salt properties and their effects remains an important research area, in particular their physiological and biological impacts. It is universally known that sodium is an essential nutrient that helps regulate bodily functions[1] such as blood pressure[2] and volume.[3] Whilst calcium along with sodium helps to shift a membrane potential in a cell which ultimately leads to muscle contraction.[4] To elaborate on various salt influences on cells there has been extensive research on their osmotic properties both within mammalian cells[5,6] and plant cells[7,8]. This generally shows the inhibitory effect increasing salinity has on cell growth and maintenance. Similarly, this inhibition at high salt concentrations has also been demonstrated in other processes such as enzyme activity[9]. The diverse effects on proteins are evident with other studies investigating salt effects on aspects such as protein folding[10], precipitation[11] and crystallisation[12]. Whilst this is abundant and valuable there seems to be a rather lacking insight into the behaviour salts exhibit on cell surface membranes and in particular the ion-lipid interactions. However recent work explores the prior in two avenues, salts solutions with monovalent and divalent cations. Early work regarding divalent cations saw the Gouy-Chapman-Stern theory being used to describe the adsorption of cations to phospholipid membranes, although it struggled to depict the nature of the adsorption[13]. Advancements in technologies have allowed for a more in depth look at this. Using high resolution x-ray diffraction, the location of the ions partition and the swelling of the bilayers was concluded[14], thereby producing a more intricate account of the divalent cation effects (fig.1). Monovalent studies include those that have confirmed that vesicles swell in salt solutions besides the x-ray diffraction analysis suggesting that the salt solutions have no effect on the membrane structure or rigidity[15].

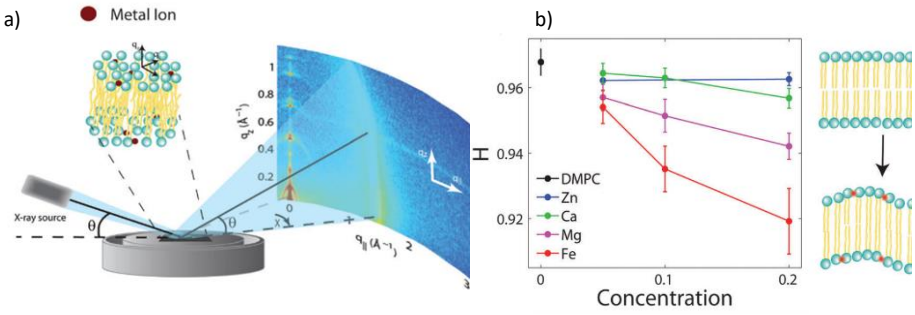

Figure 1: a) Diagram of the experimental setup used for the X-ray diffraction experiments. b) Bilayer orientation (H) as a function of salt concentration[14].

Conflicting reports have shown that salts do influence the membrane structure and have compared the strength of the interactions between monovalent cations and various phospholipid membranes[16]. Therefore, while there has been progress, the understanding of ion-lipid interactions and their mechanisms remains incoherent. A more modern approach to address this has been through molecular dynamic simulations[17], these have helped to investigate the affects ions have on the structure[18] (fig 2.) and electrochemical nature[19] of lipid membranes. This entwines into other areas such as physics and chemistry, which is encompassed in biophysics.

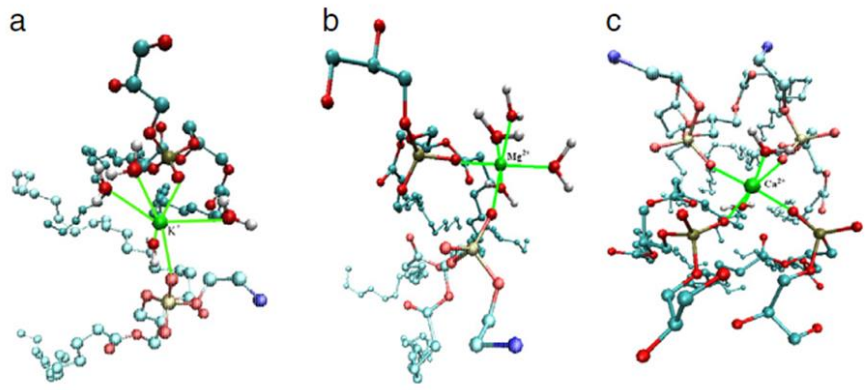

Figure 2: (a) One K^+ ion forms a complex with one POPE lipid, one POPG lipid, and four water molecules. b) One Mg^{2+} ion forms a complex with one POPE lipid, one POPG lipid, and four water molecules. c) One Ca^{2+} ion forms a complex with two POPE lipids, two POPG lipids, and two water molecules[18]

Biophysics surpasses the boundaries that more confined areas of research face by adopting interdisciplinary perspectives and applying those to biological problems. In addition to simulations and computational methods[20], biophysical research, in particular membrane biophysics, has in cooperated simple yet effective systems to elucidate the influences on lipid membranes, with the majority using model cell membranes to mimic the arrangement of lipids in natural cell membranes[21]. Another tool, electroporation[22], was developed from the previously known phenomena of 'electric modification of a cell'[23]. This reflects the electrochemistry of the cell membrane and remains important when investigating the membranes functionality. Interestingly it has been observed that the presence of salt solutions deforms giant vesicles when they undergo electroporation. This response was hypothesised to be due to ion electrophoretic forces exerted by the ions[24]. With studies like these among biophysics, it is evident that the area provides a platform for innovative ideas to address the physiological complexities at membrane level.

b) Electric Double layer:

The electric double layer was based on a model created by Helmholtz in the 1850's. It is used to visualize the interactions of charged surface in an ionic environment and remains fundamental in colloidal and surface science. Helmholtz introduced this concept through the interface of a solid metal electrode in an electrolyte solution, where two parallel layers of oppositely charged ions are formed in a fixed region[25]. Improvements on this model were made through Gouy-Chapman, who suggested that the regions of attracted ions were not as fixed as previously thought and considered their thermal motion to develop the diffuse double layer model, which considered counter-ions; this described the diffusion of ions using the Boltzmann distribution. Although it was an enhancement on the preceding theory, the Gouy-Chapman model still had limitations and failed with highly charged double layers. The Stern model combined both of the prior models to provide a more quantitative account. It suggested that ions did adhere to the solid surface which was referred to as the 'Stern layer', whilst some diffused in the diffused layer as stated in the Gouy Chapman model. It was also

recognised that the electrostatic potential at the closest point to the interface was the 'zeta potential' which provides an indication of the stability of the system. A high Zeta potential indicates the particles tendency to repel each other, contrarily a low Zeta potential would mean the particles are likely to come together[26].

The influence of electrostatic forces on ion membrane interactions can be considered in two parts: long rage columbic and short-range binding forces. Long range columbic can be explained through the Gouy-Chapman model, and has been used to describe the basic binding of cations to membrane surfaces, although modern approaches using dynamic light scattering have revealed that the binding of cations to membranes not only depends on columbic forces but on the ion concentration and availability of binding sites[27]. Short range binding forces can be explained through Langmuir isotherms. The Stern adsorption isotherm is a type of Langmuir isotherm that considers the bulk ion concentration, the bound ion density, and the electrostatic effects. This expresses the binding between ions in the aqueous phase and those bound to the membrane through an interfacial constant obtained from a Boltzman relation regarding the surface potential, which is affected by the ions in the aqueous phase and the ions that are bound to the membrane[28]. Moreover this has been applied to predict the screening ability of monovalent and divalent cations on the negatively charged lipid phosphatidylserine (PS) and illustrated how the binding and screening of cations can be differentiated[29]. The adsorption of cations such as Ca^{2+} to a charged lipid surface is electrostatically driven, and is sometimes due to a combination of the binding of a mixed ionic solute along with the unique phospholipid properties, which can lead to changes in the membrane structure such as surface patterning and curvature[13]. The competition of monovalent and divalent cation binding has previously been a complication when applying the Stern model as it depends on the stoichiometry of the ion association. For example, a 1:1 stoichiometry allows for a generalization of the model whereas a 1:2 stoichiometry requires a more intricate treatment.

With the capabilities and applications of lipid membranes becoming more varied, it is important that there is an updated understanding of the electrostatic behaviour as a lot of the functionalities are thought to be governed by electrostatic interactions. This can be done through theoretical models as seen with Lipid bilayer encapsulated nanoparticles (LBLENPs). Here the electrostatics are quantified by electrostatic potential distribution from the nano particle to the supported electric double layer found at the lipid bilayer in a salt solution. This then accounts for the electric double layer effects. The mathematical model illustrated the electrostatic mediated exchange of ions found in body fluid with the drug or cargo carried within the lipid bilayer, and it hoped to be used to reveal the ideal platforms for carrying drugs or gene for targeted deliveries[30]. Furthermore, the importance of the electrostatics on LBLENPs has been demonstrated elsewhere, an anticancer drug was integrated into a magnetic nanoparticle supported cationic lipid bilayer that was constructed around a nanoparticle core shell. The outer surface of the cationic lipid had a large positive charge density, which established a more favourable interaction leading to a more efficient drug delivery since many cancer cells have a negatively charge exterior[31] (fig 3).

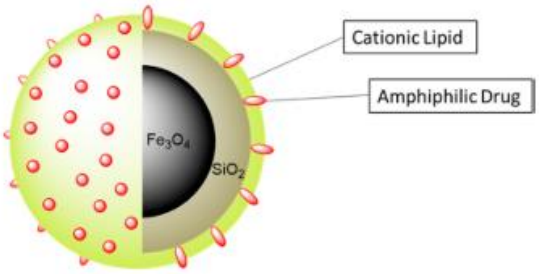

Fig.3: Magnetic nanoparticle-SLB comprised of a core–shell iron oxide–silica nanoparticle surrounded by a cationic lipid bilayer that can accommodate an amphiphilic drug[31].

c) Metal ion counterions:

The effects of metal counter ions on lipid membranes have been neglected due to the consensus that the counter ions tend to have little or no interaction with membrane surfaces, especially with neutral or zwitterionic membranes. In salts such as NaCl, it has been reported that Na^+ tends to bind weakly to the lipid head groups whilst the chloride ions form a diffuse layer with the water phase[32]. It was also suggested that the chloride ions in and other anions in general may merely compensate the charge of the cations. On the contrary, one experiment investigating alkaline cations and halide anions on a 1,2-palmitoyl-oleoyl-sn-glycero-3-phosphocholine (POPC) lipid membrane used simulations and fluorescence correlation spectroscopy (FCS) to compare other anions in sodium salts[33], and found that chloride ions can weakly interact with neutral membranes with evidence indicating that chloride ions adsorb at outer portion of the membrane at the choline region of the lipid. With the sodium ions mainly adhering to the phosphate groups an electric double layer is created unlike with CsCl or KCl. Although its potential is almost entirely compensated by the orientation of water molecules and larger anions such as I^- penetrate deeper into the membrane that smaller ions such as Cl^-. As mentioned prior it is assumed chloride ions bind weakly or not at all to zwitterionic membranes, however more recent studies use MD simulations along with experimental data to elucidate this. Isothermal titration calorimetry and electrophoretic data was used to calculate the binding constants of Na^+ and Cl^- on a POPC membrane. The experiments revealed that Na^+ and Cl^- has very similar binding constants and suggested that chloride ions bind almost as strongly as sodium ions[34].

When considering positive counter ions at the membrane surface, there appears to be competition which is similar to the previously mentioned halide ions. At an anionic membrane surface, divalent counter ions such as Ca^{2+} are more strongly attracted to the surface and will displace smaller cations like Na^+ that are bound. This is due to an ion exchange process which is an example of the entropy driven counter ion release[35] (fig 4). This differs when comparing other monovalent ions such as K^+. Potassium does bind to zwitterionic membranes but to a much lesser extent than sodium. This is due rather to the size of the ions. Sodium is smaller and has a larger surface charge and a more ordered hydration shell, therefore it has a better ability to attract water and lipid carbonyl oxygens[36]. Interestingly, when comparing the presence of chloride ions near the membrane surface, the fraction of chloride ions near the surface was higher with NaCl than with KCl. This is thought to be due to Cl^- competing with K^+ at the lipid water-interface. This doesn't appear to occur for NaCl as

sodium ions bind deeper into the surface. This correlates with KCl having a much weaker effect on the electrostatic properties of the POPC membrane than NaCl.

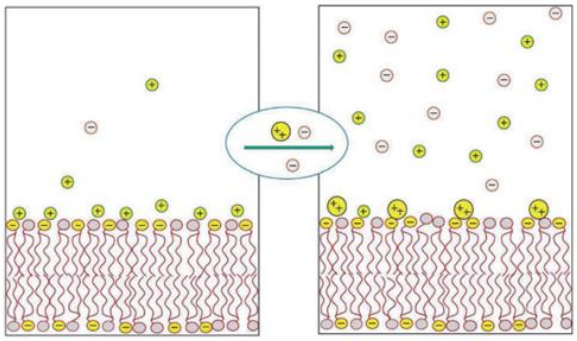

Fig.4: Illustration of the release of monovalent counterions induced by the binding of divalent cations to an acidic lipid membrane[34].

d) Cell membrane structure

Membranes are one of the fundamental structures in life, acting as a selective barrier involved in many processes such as connecting metabolic pathways and providing a foundation for cell signalling. All whilst maintaining fluidity and integrity to allow molecules to flow to and across their environments. Their functionality is a result of their structure and dynamics which are most famously known from the 'fluid mosaic model' of Singer and Nicholson, the model where the basic elements of a biomembrane structure consist of a double layer of constantly moving phospholipids as proposed previously by Danielli and Davson[37]. The phospholipids are structurally asymmetrical with one end of hydrophilic head groups and the other end consisting of hydrophobic tails. This model conformed to thermodynamic restrictions and illustrated the components of biomembranes – integral and peripheral proteins[38]. With integral proteins being more critical to the integrity of the membrane and more associated with the hydrophobic matrix and the peripheral proteins being more associated with the polar headgroups. Whilst this model has remarkably remained unchanged for the last 40 years, it is important to acknowledge that there has been important new hypotheses and experimental data appearing which expand and complement the model. These include but are not limited to: the high density of transmembrane proteins, the curvature of the membrane which depends on the geometry and mechanical properties of the membrane components and transbilayer lipid motions – the 'flip flop' motion membrane lipids can experience when under certain spatial conditions. Whilst it is described as a 'fluid mosaic model' some would describe the cartoon like structure to appear static, however it is argued that due to the many components and their degrees of freedom along with the energetic pull of the lipids, there is long term stability, which is counteracted with many destabilizing events, resulting in an overall balanced durable environment.

e) Membrane swelling/Fluctuations:

The majority of observed effects in membranes have been reported to be ion specific with less consideration for membranes in the biologically relevant liquid crystalline phase L_α, (where the lipid is more fluid in the lateral direction), and more specifically anomalous swelling and fluctuations in lipid bilayers. Anomalous swelling in bilayers and multilamella systems is frequently observed at the main phase transition temperature, although the nature of this is of debate. Various models were tried and tested with one in particular suggesting that approaching the critical temperature would result in a softer bilayer and a smaller bending modulus, K_c. This would cause an increase in repulsive forces that would result in an increase in the bilayer water thickness D_w, explaining the swelling. This was based on Helfrich proposal where a decrease in the bending modulus, K_c, would increase bilayer fluctuations. Although the model appeared reasonable, corresponding x-ray diffraction data did not support the model[39]. In later years, there has been more conclusive evidence. Neutron specular reflectivity was conducted on floating lipid bilayer systems where the results concluded that the swelling was almost undoubtedly due to the increase of the water layer between the two bilayers[40].

Helfrich originally showed that fluctuations between membranes in a certain proximity of each other would result in a repulsion interaction caused by a mutual steric hindrance. Membranes within close proximity will experience a suppression in fluctuations which leads to a decrease in entropy and an increase in free energy[41]. Fluctuations can be described as short and long range, the distinction between the two being that short range are intrinsic to a single bilayer and are often studied in molecular dynamic simulations. These are local and correspond to the disorder within a unit cell in a crystalline stack of repeating units. Long-range fluctuations occur in centre of the bilayer. These have no effect on the distribution functions and therefore do not affect the structure of single bilayers[42]. Some fluctuations include thermally induced density fluctuations and protrusions of individual molecules from the bilayer plane[43]. Thermal fluctuations have been shown using Monte Carlo simulations to induce the proliferation of pores in bilayers by overcoming an energy barrier[44]. Helfrich described in 1974 how thermal fluctuations cause the head groups in a membrane to move apart. This exposes the hydrophobic tails to an aqueous medium, the energy cost of the defects are the hydrophobic pores formed, which is essentially the energy of the exposed hydrocarbon water interface. As a result, it is energetically favourable for the lipids exposed around the hydrophobic core to re-orientate towards the pore channel to form a hydrophilic pore. The evolution of the holes is mainly determined by line tension. At large line tensions the holes become small and increase in number until the membrane becomes unstable, at reduced line tensions one hole dominates the membrane network and increases in size and shape until the network ruptures. Others have used the same simulations to conduct studies of density fluctuations in membranes at the transition region. It was found that for fully hydrated DMPC, DPPC, and DSPC, density fluctuations manifest themselves in lipid-cluster formations where the equilibrium bulk phases are occupied by clusters of the opposite phase, i.e fluid clusters in the gel phase at temperatures below the transition temperature[45]. The movement of individual lipids in the plane of a membrane known as lateral diffusion has been discussed prior with agreement that the motion of the lipid being interpreted as a ‘random walk’ or some sort of jumping model with little direct experimental or computation evidence for the mechanism. However, there has since been light shed on this through extensive atomistic simulations. Rather than a lipid moving individually in two distinct regimes, it is seen that they move in a more collective nature with their neighbour in clusters with trajectories on the tens of nanometres scale, larger than previously thought[46].

f) Hydration effect and the interactions of lipid bilayers:

A lipid membrane bilayer consists of different polar environments, with the headgroups to the glycerol groups being hydrophilic and inner membrane region of accumulated hydrocarbon chains being hydrophobic. The membrane surface refers to the hydrophilic layer, therefore this acts as the interface where interaction occurs between the membrane and surrounding water or solvents[47]. It is widely known that the behaviour of water at the lipid membrane surface of cells is related to the cells maintenance and structure[47]. It was presented that the presence of water can actually increase the stabilization of the bilayers. This was evident in DMPC bilayers, where some of the hydrogen bonded water formed intermolecular bridges between PCs which in turn formed clusters, although this differed in finite lifetimes between those in the liquid crystalline state and those in crystal form[48] (fig 5).

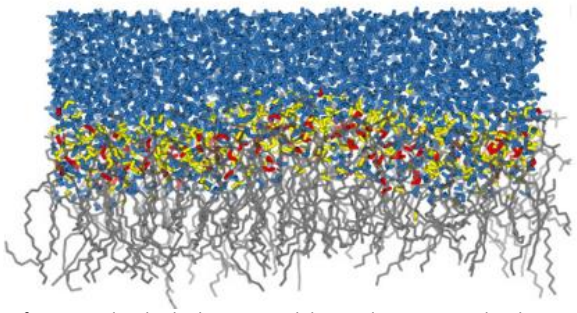

Fig.5: Different types of water molecules hydrating a PC bilayer. Blue, water molecules not H-bonded to PC; yellow, water molecules H-bonded to PC; red, water molecules bridging PC molecule[48].

With phospholipid membranes and structures such as liposomes being an appropriate biorelevant mimic to cell surface membranes it is more accessible to find a deeper insight to these processes. It is important to note that the behaviour of water molecules at substrate surfaces can be affected by the hydration characteristics and properties such as the formation of hydrogen bonds at the interface, which in turn depends on the binding position. With structures like lipid membranes the water molecules at the interface exist as hydration layers whose properties exhibit differently than those in bulk water systems. In particular, the orientation and mobility of the head groups was found to be affected by hydration by using dielectric dispersion analysis (DDA) and fluorescence spectroscopy[49]. Here it was stated that the activation energy for the reorientation of the phosphate headgroups in several zwitterionic phosphatidylcholines was reduced by hydration. As a result, this hydration would then lead to the exposure of the hydrophobic acyl chains to the aqueous bulk phase. This increased mobility of the headgroups in turn promotes the hydrophobicity of the membrane.

The difference in hydration forces between charged and uncharged lipid membranes has been subject to discussion and an investigative comparison of DMPC and DLPE has elucidated this to a molecular level description[50]. More molecular dynamic simulations were used to represent the bilayers in solvent environments. It had previously been found that the water structures around the headgroups of the bilayers had been rather different. The hydrophobic tri-methylammonium groups of DMPC resulted in formation of clathrates in water molecules, whilst the ammonium groups in

DLPE formed hydrogen bonds with the oxygens on the surrounding water. Despite these different solvent arrangements the orientational polarization was not adversely affected[51]. In addition to the study, the authors expanded with further simulations to explore the effect of water ordering on the swelling limit and hydrogen repulsions. It was found that the swelling limit for DMPC was larger than that of DLPE, this was thought to be as a result of water interactions mentioned prior. Due to the weaker inter-headgroup hydrogen bonding displayed in DMPC, the PC headgroups penetrate further into the water layer than the PE headgroups. The differing dynamics of the two bilayer headgroups were said to affect the hydration repulsions. PC headgroups move in a relatively smooth fashion whereas those of PE have to break hydrogen bonds for diffusional and rotational motions. This in turn results in little protrusion from PE headgroups from the membrane surface rendering steric interactions insignificant in this context. Overall, this results in PE membranes feeling little hydration repulsion when brought together. In comparison PC membranes experience a higher degree of hydration repulsion due to the overlap of clathrate shells on opposing headgroups along with unfavourable ordering of water molecules and entropic confinement.

g) Hofmeister series

Over a century ago, Franz Hofmeister measured the concentrations of salts needed to precipitate proteins from whole egg whites[52]. By doing so he expressed a recurring trend known as the Hofmeister series. This described how the magnitude of various ions affect protein stability and solubility[53]. The rank in order of effectiveness is shown below[54,55]:

$SO_4^{2-} > HPO_4^{2-} > OH^- > F^- > HCOO^- > CH_3COO^- > Cl^- > Br^- > NO_3^- > I^- > SCN^- > ClO_4^-$

$NH_4^+ > Cs^+ > Rb^+ > K^+ > Na^+ > Li^+ > Ca^{2+} > Mg^{2+}$

The trend remains important for biological and chemical research, for example, protein folding[56] and colloidal surface studies[57]. Despite its significance, the mechanism of the interactions of the Hofmeister ions still remains in dispute. Initially the interaction between the ions and water molecules was proposed to be due to the ions affecting the hydrogen bonding as reviewed by Collins and Washabaugh[58]. This is elaborated to suggest that the ions make or break the hydrogen bonding network. These ions are known as the Kosmotropes and chaotropes, which are also referred to "structure makers" and "structure breakers"[59]. This concept has been generally accepted and applied to the behaviour of electrolyte solutions although in recent years this has been challenged. Thermodynamic experiments have demonstrated that anions had no influence on bulk water dynamics even at high concentrations, thereby concluding that no long range structure making or breaking effects took place[60]. Other papers have expressed the importance of previously ignored dispersion potentials and their influence on the Hofmeister ion effects, although these depend on factors such as salt concentrations and the sign of the dispersion potential[61].

h) Helfrich Repulsion

The physiological characteristics of lipid membranes can be illustrated through physical parameters. W.Helfrich in particular, hypothesised that the elasticity of membranes could be described through three types of strain: stretching, tilt and curvature and their associated stresses[62]. Moreover, x-ray and neutron scattering experiments combined with molecular dynamic simulations have proved

effective in exploring the static and dynamic structure of lipid bilayers in real space by probing quantities such as electron density profiles and radial distribution functions[63].

i) Ca^{2+} vs Na^{+}

Today it is widely known that calcium and sodium ions remain of significant importance to cellular and biochemical processes, as evident through ample amounts of research. Sodium has also been shown to regulate the calcium mediated signalling in cells. N-methyl-D-aspartate receptors (NMDARs) providing a route for the uptake of calcium in neurons, however excessive uptake can lead to toxic effects and cell death. NMDARs are susceptible to Na^{+} and Ca^{2+}, since it was found that when the neurons were bathed with extracellular solution containing Na^{+}, the calcium present during NMDARs activation was reduced when the concentration of Na^{+} was reduced, suggesting that the Ca^{2+} influx is regulated by intracellular Na^{+}[64].

Calcium is required to regulate certain cellular functions. It accomplishes this due to its versatility which is achieved by its ability to display a range of spatial and temporal patterns that can be detected by various proteins[65]. This is identified as Ca^{2+} targeted proteins control mitochondrial motility and distribution along microtubules. Processes such as this require calcium ions and ATP to be interdependent, as also found in insulin secreting beta cells, where the increased ATP production leads to an influx of calcium ions which triggers exocytosis insulin secretion[66].

As described earlier, calcium's involvement with cellular membranes remains of upmost importance. To study its affects and the interactions between the two, investigations employing phospholipid membranes are often carried out as they provide an appropriate mimic to cellular membranes. Studies about these phospholipid membranes are branched into their relative net charges. For example Phosphatidylserine (PS) is a negatively charged phospholipid, and since early on it has been reported that calcium ions form complexes with the negatively charged headgroups, more specifically the phosphate ester site[67], the same report also provided evidence that the calcium phosphate complex increased the rigidity of the membrane. Later advances have illustrated through simulations how the interactions of negatively charged bilayers, DMPS and DMPG, with Ca^{2+} ions enhance the molecular packing, the results showed that the DMPS bilayer appeared more ordered than DMPG. This was thought to be due to DMPS having a carboxylate group that provided an additional site for the Ca^{2+} to interact with, this along with the fact that the DMPS can interact with neighbouring NH_3^{+} group on neighbouring lipids[68].

From prior work it is agreed that Ca^{2+} tends to bind naturally to negatively charged phospholipids. This cannot be said as such for zwitterionic lipids such as PC, where it has been shown that Ca^{2+} binds weakly[69]. However, in PS/PC lipid bilayers the adsorbed calcium ions have been shown to increase the bridging between lipid molecules, resulting in increased packing and decreased mobility of the membrane. It was also stated that other adsorption sites included the carboxylic group in the headgroup and the carbonyl group in the lipid glycerol level[70]. This work among many others included model membranes with cholesterol, where it is seen that an increase in cholesterol increases the calcium absorption despite that cholesterol having no effect on the calcium binding sites, and having no direct contact or effect on the penetration depth of the bilayer[71]. Interestingly sodium has an opposite relationship to cholesterol than that of calcium. Here an increase in cholesterol results in a decreased Na^{+} adsorption, due to the cholesterol occupying the lipid

headgroups thereby decreasing the ion binding sites. It is also stated that the increase in cholesterol increases the hydrophobicity in the membrane which further diminishes the membranes affinity for cations[72]. Additionally, with zwitterionic membranes, the surface interactions of sodium and calcium differ slightly since the adsorption of sodium mainly depends on the amount of headgroups available while the number of adsorbed calcium cations depends more so on the available surface area.

Sodium has often been used in comparison to calcium in the study of the asymmetrical bilayers. It is often reported that it has a weaker interaction but none the less still has some impact on mixed bilayers such as DPPC/DPPS[73]. Similar to calcium it appears that sodium also binds to both the phosphate group and the carbonyl group although evidence suggests there is a preference for the phosphate group. In zwitterionic monolayers such as DPPC, electron densities profiles have shown there is little interaction between Na^+ ions and the lipids, and that sodium and chloride ions would prefer to distribute themselves homogeneously in a water subphase, but in negatively charged lipid monolayers such as DPPG sodium readily diffuses in the lipid head group area[74]. In other electron density profiles such as those of anionic POPG, Na^+ has a tendency to remain near the lipid headgroups (due to electrostatic interactions) and is in competition with the electrostatic repulsion the ions experienced between the Na^+ ions, along with their thermal motion and the energy compensation from hydration. This paper also used these density profiles to describe how some of the Na^+ ions were found to be located in the water phase beyond the phosphate groups. Yet as the distribution of sodium ions is affected by the surface potential of the negatively charged lipid surface, they prefer to interact with the ester groups rather than the phosphate groups[75]. Coordination numbers were used to confirm this, and the numbers of the Na^+ at the ester region at the water membrane interface were at a maximum. Here two or more lipids can bind to each other via sodium as ion bridges.

j) Neutron Reflectometry with Lipid membranes

Neutron reflectometry makes for an ideal technique to study membranes and other soft matter systems due to its non-destructive nature and long penetration depths. Also, it is sensitive to light elements such as carbon, nitrogen, oxygen and deuterium, as they strongly scatter neutrons. This makes the technique useful for studying biological samples[76]. Neutron reflectometry has mainly been utilized to determine the structure or components of lipid bilayers with the majority focusing on supported bilayers with additional techniques[77]. The support systems used with bilayers has been subject to comparison, as even though most provide stability, they display limitations such as localized pinning and frictional drag which hinder advanced applications. To accommodate this the development and incorporation of nano-porous and nano composite thin films has been demonstrated to be promising in the support of bilayers, as they require no prior surface treatments and allow for the self-assembly of well packed bilayers, mainly in contrast with alumina supports[76]. This technique has also been extended and used in the analysis of bio-interfaces and thin film structures[78]. This included the investigation of the properties of lipid bilayers under sheer liquid stress and the effects of various pH environments on the separation of lipid bilayers and thin film substrates. Both provided significant insight into potential biomedical applications and demonstrated the versatility in the method.

k) QCM with lipid membranes

A quartz crystal microbalance (QCM) is a surface sensitive device capable of detecting mass changes on a molecular scale. It has a wide range of applications in chemistry, biology and material science and has been applied frequently to study phenomena at various interfaces. The smart device operates on a piezoelectric quartz crystal which oscillates at a fundamental frequency as a result of an AC voltage[79]. Deposited species cause mass changes which in turn cause a change of frequency, the specific mass change is then calculated through the Sauerbrey equation. The device is often paired with dissipation monitoring (QCM-D), which operates the same as QCM but measures the energy loss along with mass change to provide insight on the rigidity of the species deposited, allowing for viscoelastic modelling of the data as well. It is often utilized as it can collect data in real time, which was demonstrated in a review probing the interactions between nanoparticles and supported lipid bilayer (SLB) systems. This also included the formation and characterization of the SLB. Various studies were described such as the effect of solution chemistry on the interaction of nanoparticles and SLB's and the effect of environmental and biological changes on the same interaction. When the QCM technique is combined with another such as Neutron reflectometry, it provides an accurate and effective method for studying structure and adsorption in membranes. This has proven to be advantageous in neuroscience, where the complementary techniques were used to study the adsorption of a protein, related to Parkinson's disease, to supported bilayers[80]. Interestingly, the results implied that the protein, α-synuclein, was adsorbed in the headgroup region of anionic lipid bilayers but did not penetrate deeply into the hydrophobic acyl chain region, much like most of the literature describing adsorption into membranes. It was also found that the association of α-synuclein to the membrane was mostly electrostatic in nature, with little dependence on the headgroup separation.

l) Recent studies in salt/membrane interactions

Biomembranes remain some of the most important biological structures, consisting of a double layer of phospholipids which overall acts as a cell barrier[37]. There is an abundance of information regarding their biological processes including the role of ions such as gating ion channels[81] and transporting across membranes[82]. This being said, developments in membrane and nanotechnology proved advantageous when investigating this. Ions in aqueous solutions are known to modify the membrane structure and dynamics. In recent years AFM (Atomic force microscopy)-based Force-Spectroscopy (AFM-FS) has been used to highlight how cations enhance the mechanical stability of a phospholipid bilayer[83](fig 6 and 7). These advances have also become more established in industry. Areas have been vast and have included those in the food sector, and those in water treatment[84] where a method common to both is the monitoring and control of biofouling[85]. Biofouling of anion exchange membranes with red wine was explored, where the specific components in wine that cause the membrane deterioration were identified using techniques such as ATR-FTIR spectroscopy, AFM, and voltammetry[86]. Nanofiltration membranes have been utilized in their potential in water treatment, where it was found that controlling the salt and photoelectrolyte concentrations affects membrane pore size which could lead to a more selective membrane separation process[87].

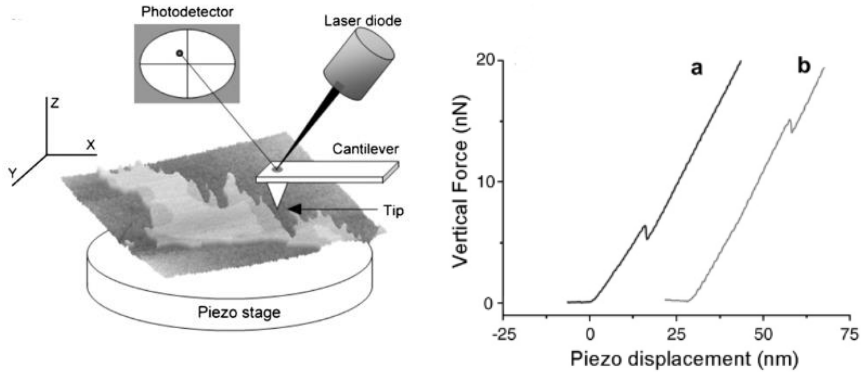

Fig 6: Schematics of the experimental AFM set-up. The bilayer is elastically deformed by the cantilever tip and the tip ruptures the lipid bilayer, thus becoming in contact with the mica substrate64. Fig 7: a) DMPC bilayer on mica in 10 mM HEPES, pH 7.4 buffer solution. b) DMPC bilayer on mica in a 10 mM HEPES, 150 mM NaCl+20 mM $MgCl_2$, pH 7.4 buffer solution. 'In the absence of ionic strength in the solution, the DMPC bilayer breaks on average at forces~4 nN, whereas under high ionic strength conditions the bilayer breaks at forces as high as~15 nN.

4) Scope of the study

Salt interactions and influences on lipid membranes has been subject to discussion and study for several years. This being said, research regarding zwitterionic membranes has been less favoured. Also, the majority of studies that attempt to investigate the behaviour of membranes under salt influences have been through simulations. Therefore, the following attempts to provide physical evidence of these salt interactions through physical experiments, more specifically using a quartz crystal microbalance, Langmuir pressure isotherms, and neutron reflectometry. Sodium chloride and Calcium chloride were used for comparison and both monolayers and a single bilayer were included in the study.

5) Materials and Method

a) Materials:

Sodium Chloride (NaCl) – Sigma Aldrich, Lot No: SLBZ8529. Ammonium Hydroxide (NH_4OH) – Sigma Aldrich, Lot No: STB69680. Hydrogen Peroxide Solution (H_2O_2) – Sigma Aldrich, Lot No: STBJ1604. Chloroform ($CHCl_3$) – Fisher Scientific. QCM Crystals (Quartz) – Novaetech. Non deuterated 1,2 – dipalmitoyl –sn-glycero-3-phosphocholine (DPPC) – Avantipolar lipids. Ultra-pure water.

b) Methods:

i) Quartz Crystal Microbalance:

- RCA Cleaning:

  Ammonium hydroxide, hydrogen peroxide and ultra-pure water in a glass beaker in a 1:1:5 ratio. Attached an electronic thermometer to a heating mantle. QCM crystal placed in a PTFE

holder; this then placed in the beaker full of RCA cleaning solution and heated to 70° - 80° C for 10 minutes. This was allowed to cool to room temperature and rinsed with ultra-pure water. If not in immediate use, then the crystals were stored in beakers of ultrapure water covered with parafilm. When in use the QCM Crystal placed on lint free tissue to remove excess solution then placed into QCM.

- Preparation of lipid:

  0.01g of DPPC in 10 mL of chloroform, evaporated with nitrogen gas, re-suspended in 10 mL ultra-pure water, sonicated for at least 15 minutes.

- Preparation of NaCl and $CaCl_2$ solutions:

  0.5846g NaCl in 100 mL ultra-pure water to produce 100mM. Diluted using Eppendorf pipettes to produce 50, 20, 10, 5, 2, and 1mM. 1.4701g of $CaCl_2.2H_2O$ in 100mL UPW to produce 100mM. Diluted to create 50,20,10,5,1 and 1mM.

- QCM Setup and Runs:

  The QCM device is attached to a computer via USB connection. Th system includes two major parts: digital and analog. The digital part records the frequency of the signal and is also responsible for connecting the crystal to the analog part of the system[88]. When the signal is connected to the analog part of the circuit the envelope of the damped sinusoidal is processed by the envelope detector, and then converted to digital. Any switching or start of the signal is controlled by the computer. The gold quartz crystal is placed on the electronic console and the resonance frequency of the oscillator is monitored by the 'Open QCM' software. The QCM is integrated in a fluid circuit consisting of the cell which contains the crystal and oscillator. Two tube were then attached to the QCM lid and connected to a syringe pump. The interval times were controlled by the syringe pump and after each run the QCM was left to rest for at least 5 minutes to allow the run line to plateau on the Open QCM software.

  The change in frequency calculated by the Open QCM software is proportional to the mass detected by the electrode as described by the Sauerbrey equation:

$$\Delta m = \frac{A\sqrt{\rho_q G_q}}{2{f_o}^2}\Delta f$$

Eq.1 Sauerbrey equation connecting a change in mass to change in frequency

Δm = Change in mass (g)
Δf = Change in frequency (Hz)
f_o = Resonant frequency (10^6 Hz)
A = Area of the gold electrode (cm^2)
ρ_q = Density of Quartz (2.648 gcm^{-2})
G_q = Sheer modulus of Quartz crystal ($2x10^{-11}$ $gcm.s^{-2}$)

Area per molecule:

1. Mole of lipid x Avagodro's constant = Units in bilayer
2. Units in bilayer / 2 = Units per area of electrode
3. Area of electrode / Units per area = Area per molecule (cm^2)

Table 1: QCM run plan used:

Substance	Volume (ml)	Flow rate (mL/Min)
UPW	10	0.5
Rest	-	-
Lipid (DPPC)	3	0.35
Rest	-	-
UPW	10	0.5
Rest	-	-
NaCl (1 mM)	3	0.35
Rest	-	-
NaCl (2 mM)	3	0.35
Rest	-	-
NaCl (5 mM)	3	0.35
Rest	-	-
NaCl (10 mM)	3	0.35
Rest	-	-
NaCl (20 mM)	3	0.35
Rest	-	-
NaCl (50 mM)	3	0.35
Rest	-	-
NaCl (100 mM)	3	0.35
Rest	-	-
UPW	6	0.5
Rest	-	-

ii) Neutron Method:

Instrumentation:

Measurements were conducted at ISIS Neutron Facility, on the high flux spallation source SURF neutron reflectometer. A 25K hydrogen moderator was to slow the neutrons to the required wavelength. An incident neutron wavelength between 0.55 Å -6.8 Å was achieved by extracting the neutrons using a super mirror guide inclined 1.5° below the horizontal with a chopper array 6m from the target. A double slit geometry ensured a narrowed primary beam.

A silicon crystal substrate positioned on a high accuracy two axis goniometer to a 0 0 1 plane and was polished to 3Å RMS.

A low background ^{3}He point detector was used with the background detection further minimized by another two slits in the flight path between the sample and detector.

Use of Langmuir for sample preparation:

Langmuir trough

The Langmuir trough experiments were carried out using 'Nima' software. Before use, the Langmuir trough was cleaned thoroughly with Kimwipes soaked in chlororform.

Langmuir-Schaefer deposition

To prepare the bilayers for neutron analysis a Langmuir trough was used to deposit the bilayers to a solid substrate. A combination of Langmuir Blodgett and Langmuir Schaeffer depositions were used**.** The lipid was dissolved in chloroform and deposited onto the trough. Then a DPPC monolayer was compressed to a pressure of 40 mNm^{-1} at a barrier speed of 50 cm^{2}. This was held at this pressure whilst the substrate was pulled through the monolayer at a speed of 4mm/min followed by a Langmuir-Schaeffer (LS) deposition. This was to maintain the deposited layers as a Langmuir Blodgett deposition would have removed them. During the Langmuir deposition the hydrophobic substrate was held horizontal to the water surface and slowly lowered through the monolayer into a sealed sample cell under water in a low exchange volume solid-liquid neutron cell, with temperature controlled using water circulation via heating plates from a water bath. All data presented was collected on the SURF reflectometer at three angles 0.35°, 0.8° and 1.8°, which were spliced together and cut at 0.3 $Å^{-1}$ in quartz for clarity.

Analysis of Data:

Analysis of neutron data was carried out using Rascal, a reflectivity modelling software used within MatLab. This was used to fit multiple data sets at once according to a model SLD profile. These models were created to mimic the bilayer system according to the substrate, see fig. 7 and 8. The profile was formed using MATLAB by using custom layers starting from the substrate surface (silicon crystal). The profiles can be seen below in Tables 2 and 3. The layers included parameters that can be adjusted within physical boundaries, including thickness, roughness, hydration, and scattering length density (SLD) these parameters were applied for each layer in the bilayer. Once an SLD profile was built, an Abeles matrix formalism was used to compare the profile to the reflectivity data to form a goodness of fit. In order to fit the data the values of the layers within the model were altered until chi squared could be minimized and visually the fit looked right on the SLD profile.

The errors presented are the result of Monte Carlo error analysis within Rascal, known as 'bootstrap errors'. This approach to estimating errors involves finding the distribution values for each parameter fitted as a function of the initial starting values. For all the errors presented the minimization was repeated 1000 times with randomized starting values fitted to a randomized number of points within the raw data, the standard deviation of possible values for each parameter based on this was then found.

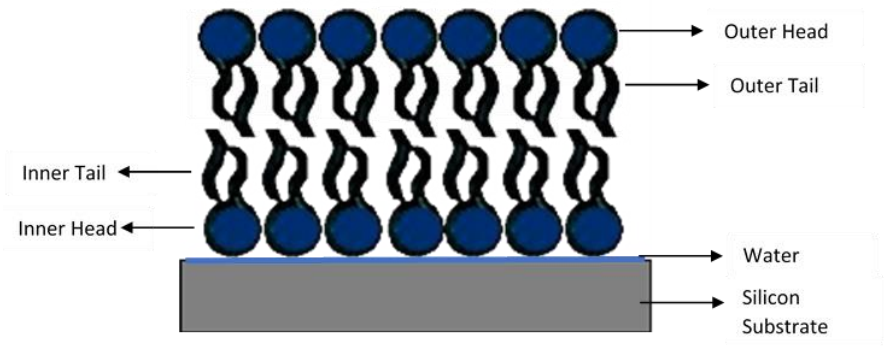

Fig. 7 Labelled model of floating bilayer adhered to a silicon substrate

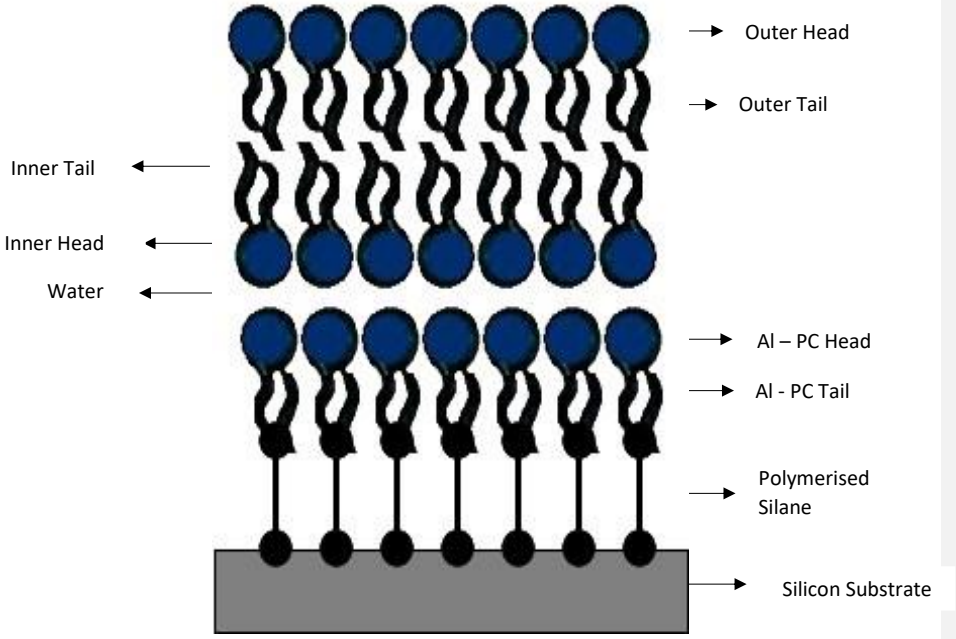

Fig. 8: Labelled model of a bilayer deposited on a al – PC SAM.

Table 2: Model used to fit adhered bilayer neutron data

Bulk In	Silicon
	SiO_x
	Water
	Inner Head
	Inner Tail
	Outer Tail
	Outer Head

Bulk Out	D_2O

Table 3: Model used to fit the floating bilayer neutron data

Bulk In	Silicon
	SiO_x
	Polymerised Silane
	Al - PC Tail
	Al - PC Head
	Water
	Inner Head
	Inner Tail
	Outer Tail
	Outer Head
Bulk Out	D_2O

iii) Langmuir Isotherms:

Hydrogenated DPPC monolayers were spread on a Langmuir with the varying $CaCl_2$ concentrations: 0 mM, 1.25 mM, 5 mM, 20 mM, 100 mM. These were dissolved in the H_2O subphase and kept at a constant temperature of 20°C using heating plates. The lipid was then left for 15 minutes to allow the solvent to evaporate. To carry out the isotherm, the Langmuir trough was compressed at 50 cm^2/min until the monolayer collapsed. This was repeated 3 times for each of the $CaCl_2$ in the subphase.

6) Results and discussion:

a) QCM Data

i) NaCl:

Here a QCM was used to quantify the deposition and adsorption of DPPC bilayers onto a gold surface, then further quantify any mass changes due to the addition of metal salts, in this case NaCl and $CaCl_2$. The total injection time for the initial NaCl run (fig. 9) was 4 hours and 48 minutes with DPPC being injected at 4538 seconds. From the DPPC rest there is a decrease in frequency of -236.9 Hz indicating that the lipid has been adsorbed to the surface. This value was used to calculate an area per molecule of 45.5 Å which falls within the range of area per molecule for DPPC as previously seen with H_2O[89]. When comparing the individual concentrations, it is more applicable to compare the frequency losses to the UPW rest after the lipid was deposited. This then disregards the lipid lost to the UPW wash. Initially there was a decrease of $2.14x10^{-8}$ g after 1mM of NaCl was injected. Then there was a very little mass change of $7.6x10^{-9}$ that followed after 2mM was injected. However, this trend of a decrease in mass appears to become larger with an increase in concentration with this being most prominent between 20-100 mM. The frequency change relative from the UPW rest after the lipid for 20 mM was -164 Hz, resulting in a 2.1×10^{-7} g mass loss, this was followed by the largest mass loss of 3.3×10^{-7} g at 50 mM, and then finally a slightly less mass loss of 3.1×10^{-7} g at 100 mM. The overall mass loss at the end of the run after 100mM was $2.67x10^{-7}$g.

The total injection time for the second run for NaCl (fig. 10) was 5 hours and 1 minute with DPPC being injected at 1727 seconds. From the injection of DPPC there is again a decrease in frequency of – 77Hz indicating there has been some adsorption occurred. This value was then used to calculate an area per molecule of 71.8 Å which is larger than the range of 40-50Å that was stated in previous literature. Much like the previous NaCl run there is an overall trend of increase in frequency meaning a loss of mass over the entire run. The mass loss over the entire run after 100mM was $2.43x10^{-7}$g, quite similar but just lower than the loss experienced in the first run. The initial mass loss at 1mM NaCl appears to be greater at $7.24x10^{-8}$ g than that of the previous run. There appeared to be a larger difference in mass loss of $2.11x10^{-8}$g between 1-2mM when compared to the prior NaCl run, and when comparing the mass loss between concentration during the entire run, there appears to be a more gradual increase in frequency and therefore mass loss. This is evident when the mass losses between each concentration for the second NaCl run stay within 2 - $7x10^{-8}$g from 0-100mM, whereas the mass loss for the first run is slightly more erratic with the losses being around 2 - $9x10^{-8}$ between 0 – 10mM, then increasing to 2 - $3x10^{-7}$g between 20-100mM. It should be noted that both of the NaCl runs display a decrease in mass at 20 - 100mM. The first run has a decrease of $1.9x10^{-8}$g, whilst the second decreased by $5.62x10^{-8}$g, the fact that this trend occurs for both runs suggest the same or at least similar incidence is occurring. It is likely there is a disruption in the bilayer, and as the concentrations increased there is an increasing fluctuation. This leads to a further disruption in the lipid and as a result parts may escape into the solution leading to a mass loss. It should be mentioned that lipid loss to the solution may not occur in an even fashion as it likely that there was not a complete uniform deposition of the lipid in the first place and the lipid may have absorbed to the surface with aggregates. Therefore, further QCM runs considering concentrations above 100mM would be useful and significant in order to elucidate the behaviour of the lipid in this environment.

ii) $CaCl_2$:

Unfortunately, due to faults in the QCM system and software, a complete run from 0-100mM could not be completed for $CaCl_2$. However, a run from 0-20 mM (Fig 11) and 50mM (Appendix 1) were achieved after some adjustments. The run for 0-20mM was completed in 3 hours and 36 minutes, with the DPPC lipid being injected at 3983 seconds. Once the lipid was deposited there was a frequency decrease of 62Hz which was then used to calculate an area per molecule of 89Å which is nearly double the range of 40-45Å as stated in the literature. This may indicate perhaps multiple layers deposited of aggregates which is likely to occur. Like the NaCl runs there is an overall decrease in frequency and therefore loss in mass overall. This tends to occur less erratically than the first NaCl run. Over the entire run the mass losses between concentrations 0-20mM remain between 2 - $8x10^{-8}$ g. The largest mass loss occurs between 1-2mM with a loss of $3.23x10^{-8}$ g. Unfortunately, due to faults in the QCM system it is impossible to compare the higher concentrations of $CaCl_2$. Overall, from 0-20mM $CaCl_2$ there is a total mass loss of $2.84x10^{-7}$ g, which is slightly above the mass losses for the entirety of both NaCl QCM runs. Interestingly, for both NaCl runs there was an increase in mass between 20-100mM, as we are unable to achieve results for above 20mM for the $CaCl_2$ effectively this would warrant further investigation. Also, when looking at 50mM there is still a significant mass loss of $2.42x10^{-8}$ g, where repeated runs would be needed to see if the trend continues with higher concentrations.

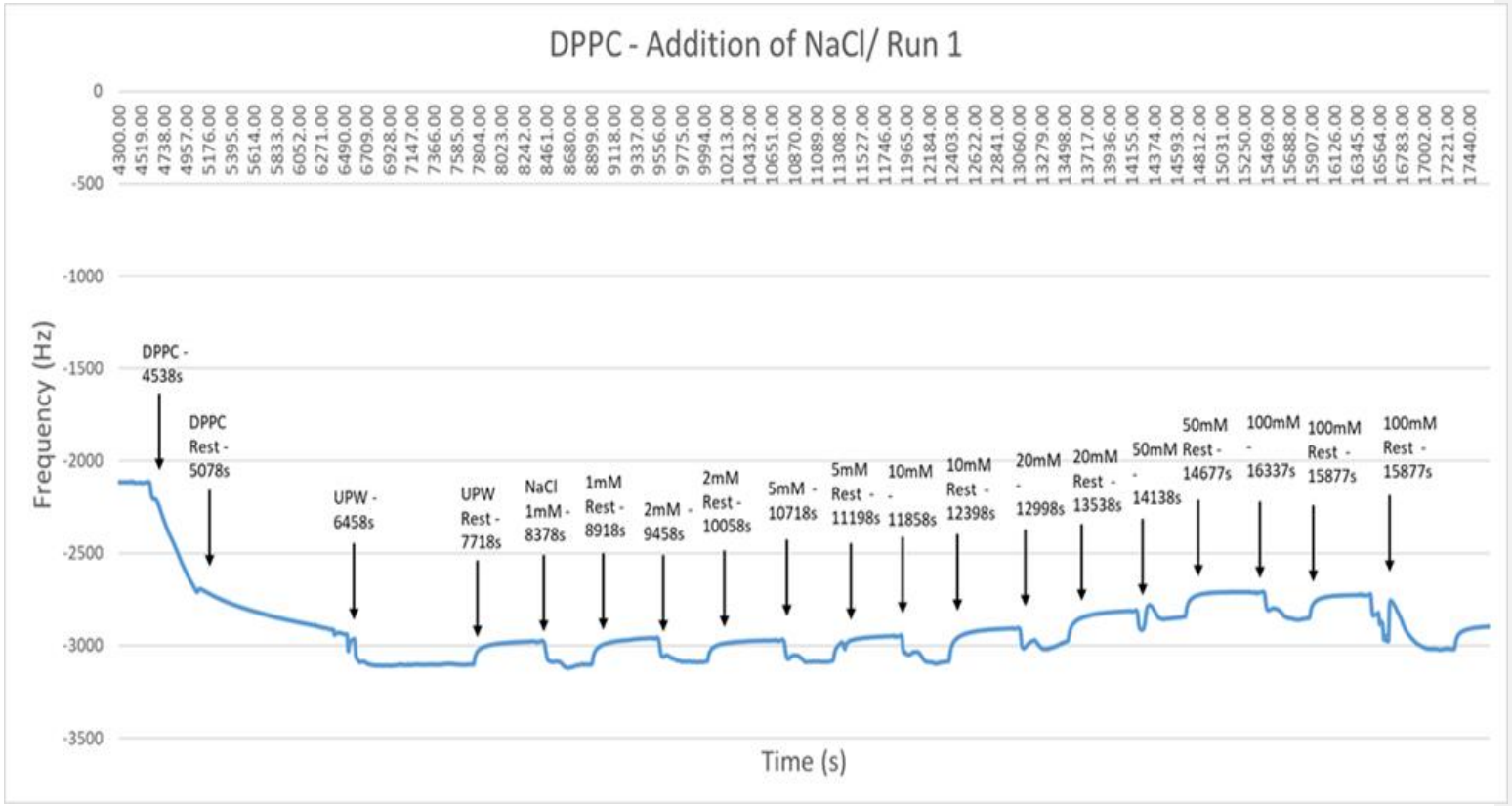

Fig 9: DPPC QCM first run with the addition of NaCl in increasing concentrations from 0mM to 100mM.

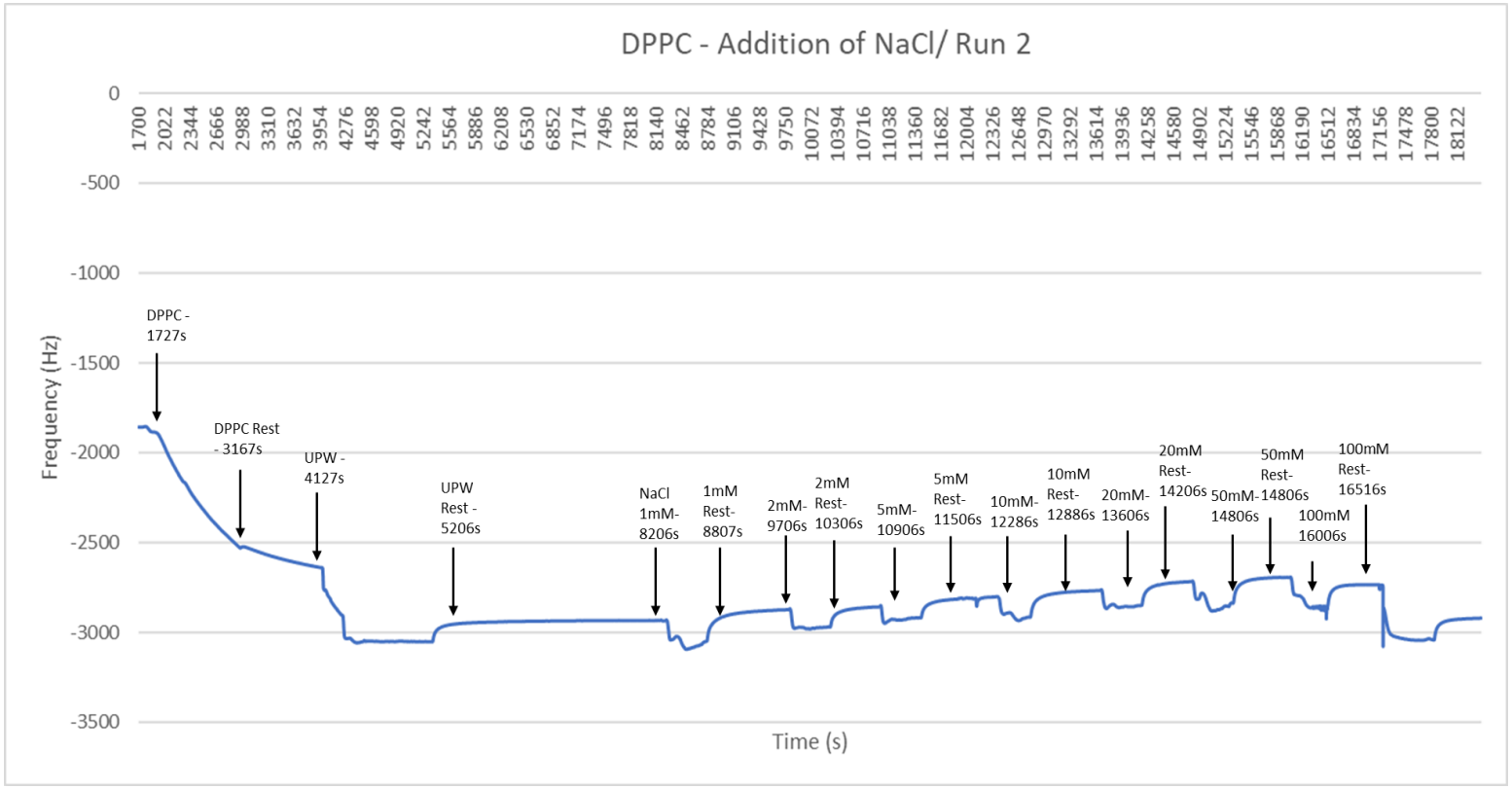

Fig 10: Second DPPC QCM run with the addition of NaCl in increasing concentrations from 0mM to 100mM.

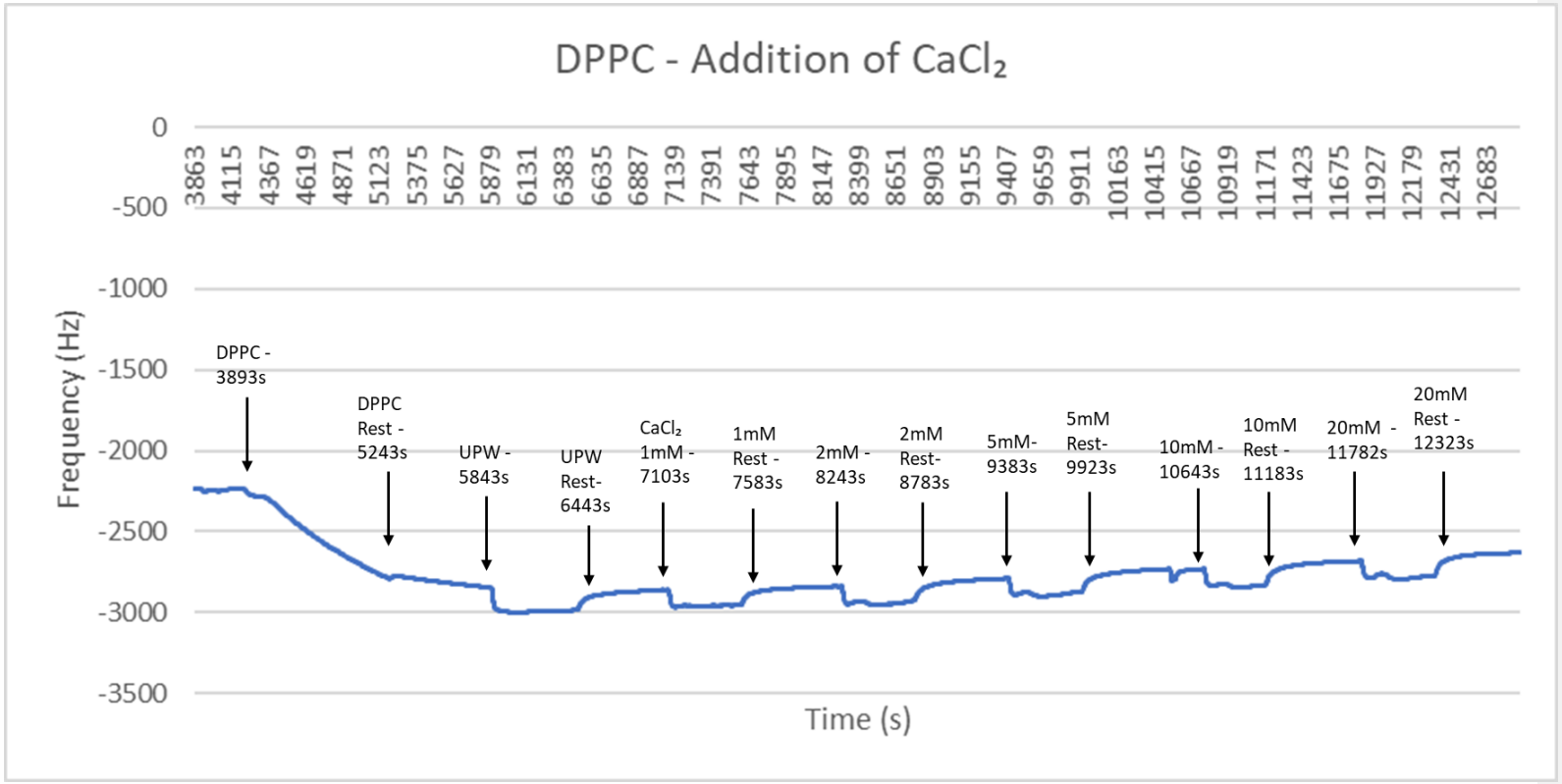

Fig. 11: DPPC QCM run with the addition of $CaCl_2$ l in increasing concentrations from 0mM to 20mM.

b) Isotherms

i) $CaCl_2$:

The isotherm shown in figure 12 illustrates the behaviour of the hDPPC monolayer leaflet under various $CaCl_2$ concentrations. Initially at 'lift off' or low surface pressures of 0 – 10 m/Nm there is generally a decrease in area per molecule for all $CaCl_2$ concentrations, with 100 mM rand 1.25 mM reaching the lowest and decreasing below 90Å, whilst water appears to decrease from values above 100Å. As the surface pressure increases towards 10 – 20 m/Nm, there is a plateau between 60 – 75Å which indicates the co-existence of phases. Here the effect of the various $CaCl_2$ appears to be similar with little change occurring at the monolayer, although the area per molecule at 20 mM begins to decrease at a greater extent than 5 mM. As the surface pressure increases towards the condensed phase from 20 – 40 m/Nm, there is a sharp decrease in area per molecule, with the largest difference occurring between 5 and 20 mM, and with 5mM decreasing at a higher area per molecule than 20 mM. This implies that the monolayer at 5mM is the least stable, as there is a decrease in area per molecule at higher concentrations. This is most likely due to Ca ions bridging between the lipid molecules, as concluded from prior literature; Ca has been shown to increase the bridging between molecules resulting in increased packing and decreased mobility making the monolayer more rigid and less stable. This bridging is said to occur between the phosphate headgroup with other adsorption sites including the carbonyl group in the lipid glycerol level[74,75]. Above 5mM there is a decrease in area per molecule at the same surface pressures, which implies that the lipid monolayer is disrupting, this could be a result of saturation from the increasing salt concentrations which may cause the lipid to collapse through repulsion of the cations or electrostatic repulsion in the lateral direction from the closely packed headgroups.

ii) NaCl:

Figure 13 shows another isotherm for hDPPC however this shows the effect on the monolayer under various NaCl concentrations. At 'lift off' from 0-10 m/Nm surface pressure there is again a decrease in area per molecule across all NaCl concentrations, however this occurs at lower values in general around 50-70Å. This decrease is also more abrupt than that in the isotherm of the $CaCl_2$ concentrations. From 0 – 10m/Nm there is a decrease in area per molecule where the most significant point being that 5 and 100mM overlap 20mM, which is due to the higher surface energy in this phase. Here the liquid phase is stabilising however there is also potential for disruption of the phase transition. As the surface pressure increases towards 10-20 m/Nm there is a plateau where there is a co-existence of phases, however unlike the prior isotherm in figure 11, this once again occurs more abruptly and interestingly the 100mM NaCl concentration occurs at a higher surface pressure than all other concentrations, whilst 20 mM remains at the lowest surface pressure during this period. The kink that appears for 100mM at around 35Å is likely a result due to the collapse of the lipid. There is also no overtaking of concentrations like that which occurred with the 20 mM $CaCl_2$ concentration over 5 mM. As the surface pressure increases towards the condensed phase, there are more similarities between the isotherms, with 20 mM reaching at a lower area per molecule than 5 mM, and 100 mM remaining at the lowest area per molecule although this appears in a more irregular fashion than 100mM $CaCl_2$.

In regard to the difference in behaviour of the monolayer under the two salt environments, the comparison between 5 and 20 mM is the most significant. The reason for this is that it could imply

evidence of the possible saturation or monolayer disruption due to different salts. As stated previously 5 mM overlaps 20 mM $CaCl_2$ indicating possible Ca – ion bridging occurring between the lipid, conversely, this does not appear in the isotherm for the NaCl concentrations. This complies with previous literature that shows that sodium tends to have little interaction with lipid and that sodium and chloride ions would rather distribute themselves in the water subphase, especially with zwitterionic lipids[79]. Due to the zwitterionic nature of the lipid, there is less electrostatic repulsion experienced by the DPPC heads. This would mean the lipid would be more tightly packed with less lateral mobility, which then puts emphasis on the effect of the cations. Therefore, there is more confidence in the idea that Ca ions cause bridging between the lipids over sodium due to fact that the isotherm for $CaCl_2$ and NaCl differ in where the lipid remains more stable over increasing pressure with $CaCl_2$ up until concentrations above 5 mM.

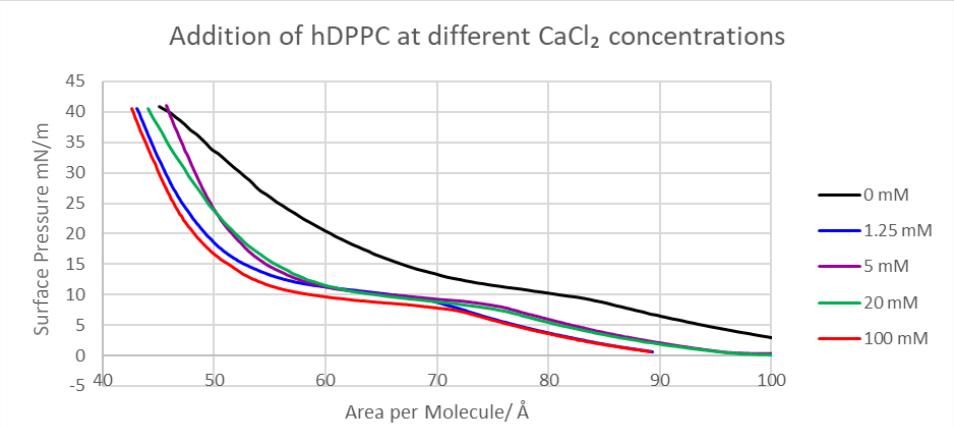

Fig 12: Isotherm showing addition of $CaCl_2$ to a hDPPC monolayer leaflet.

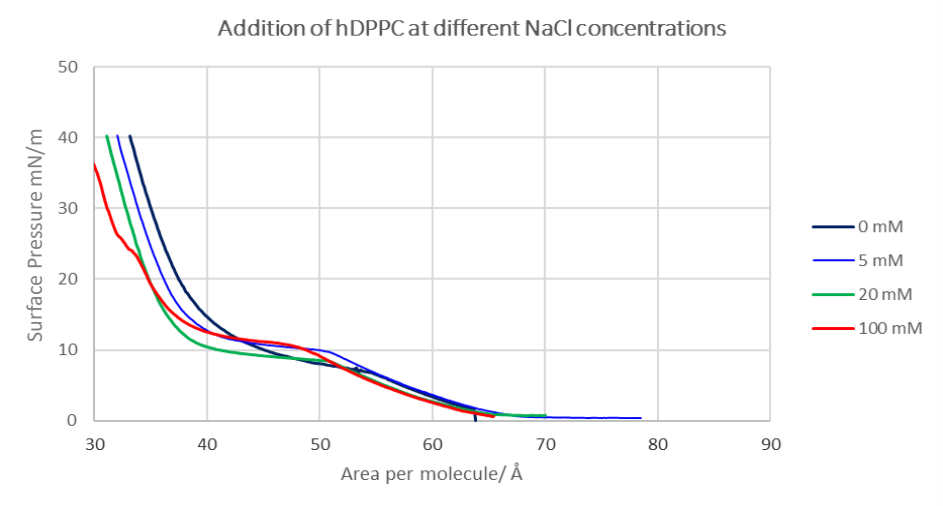

Fig 13: Isotherm showing addition of NaCl to hDPPC monolayer leaflet.

c) Neutron Reflectometry

Neutron reflectivity data (figure 14) and the SLD profiles (figure 15) for the hDPPC bilayer were obtained in D_2O, H_2O and Silicon matched water (SMW), presented below. The fits were conducted using Rascal and the parameters determined from these fits. The values in Table 4 below represent some of the parameters measured for the bilayer. The thickness values for the hDPPC heads and tails are similar to those reported in previous literature[90,91]. This and the SLD profile indicate that a bilayer has been deposited successfully. There was an issue with the water measurement as the SLD value is higher than the previously reported -0.56. This may be due to a poor exchange and possibly some D_2O in the water. Looking at the hydration values, the silicon oxide layer has a reported 26% hydration, which appears to be relatively normal however it may suggest that gaps occurred within the layer. The head hydration remains the highest at 64%, which is again expected as the heads are hydrophilic and remain on the outside of the bilayer. The hydration for the tails implies that the coverage is low, yet enough to increase the roughness compared to the other layers, although the fact that the tails are thicker than the heads also contribute to their increased roughness. It should be noted that this assumes that the bilayer is symmetric.

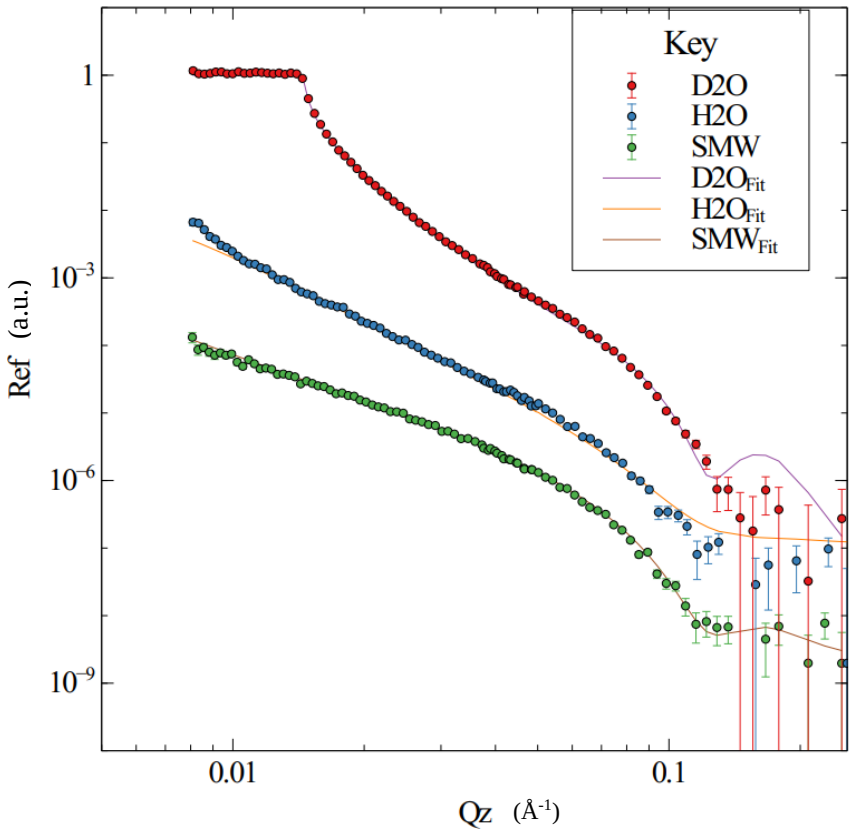

Figure 14: Neutron reflectivity data sets for hDPPC in D_2O, H_2O and SMW

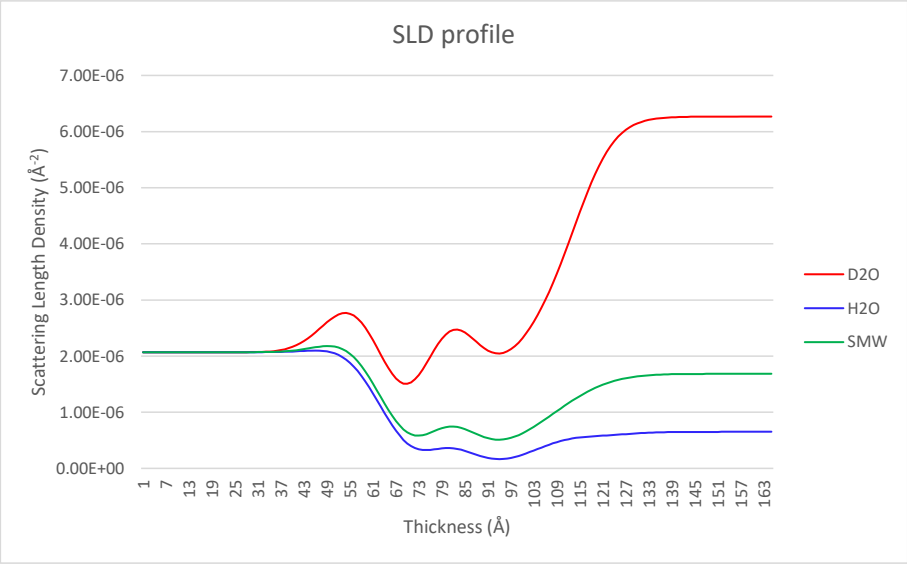

Figure 15: SLD profile for hDPPC in D_2O, H_2O and SMW

Table 4: Value for parameters obtained for hDPPC

Layer	Thickness/Å	Roughness/Å	Hydration/%
Silicon oxide	13	9	26
Water	13	7	5
Head	7	7	64
Tail	12	12	27

Neutron reflectometry data was collected from a single bilayer of hDPPC by exchanging the subphase for 1,5,20,50, 100mM and 1M $CaCl_2$ in D_2O. Fig 16. illustrates that after fitting the SLD profiles, it is evident that the bilayer remained unaffected by any application of the salt concentrations. This is illustrated through how the scattering curves overlap precisely, suggesting that the interaction between the salts and bilayer was minimal or non-existent. Any loss of lipid witnessed, such as that implied in the prior experiments in this study, would be beyond the detection of a neutron reflectometry experiment as the resolution is too high. As there was little to no interaction, it was likely that the cation-phosphate interaction was too weak to remove one of the solvating water molecules from the phosphate group[92]. Those that did bind however, were indicated to be affected by the average orientation of Ca^{2+} bound to the phosphate group and the extinction coefficient of the PO^{2-} group when the phosphate calcium complex formed[93].

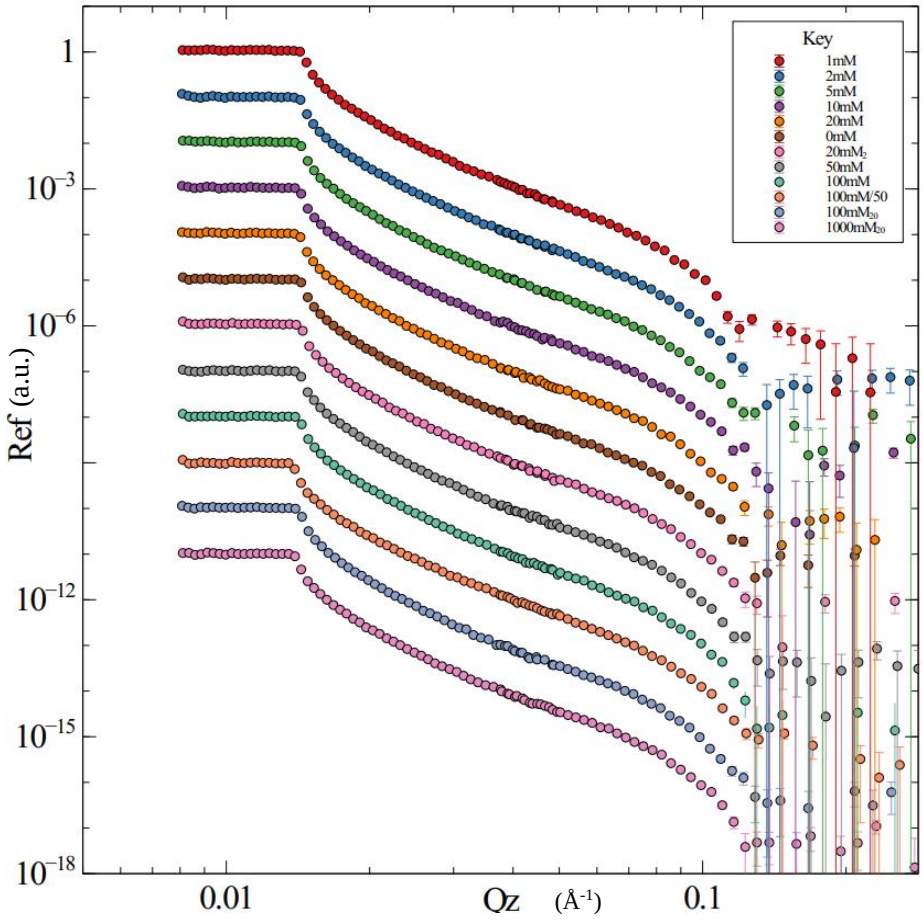

Figure 16: Reflectivity data for hDPPC under $CaCl_2$ concentrations 0-1M.

i) al – PC SAM

When performing neutron reflectometry on floating bilayers, a self-assembled monolayer (SAM) with a polymerised chain attached was first formed. A single floating bilayer was deposited onto a functionalised silicon substrate from a lipid monolayer using a Langmuir Blodgett. This al-PC SAM was incorporated as the model is more robust and assures a floating bilayer. The data presented below regarding these was also collected at SURF and was fit using Rascal. The model used for Rascal was derived using certain parameters; 'Waters per Head', Area per Molecule (APM), Global/local roughness. For the al-PC, roughness was considered as an overall parameter coupled across all bilayer interfaces. These parameters are discussed below. From figure 17 it is illustrated that the SAM and polymerised al-PC was successfully deposited and the values from the neutron data (Table 5) confirm this as they correspond to those found in literature for the gel phase at 20°C. It is

important to note that these values vary with temperature and will therefore be different for the fluid phase at 50°C. It was important to consider the interaction of al-PC SAM with $CaCl_2$, which is illustrated in figure 18. Table 5 displays the values collected from the reflectivity data for the al-PC SAM alone and under 10mM $CaCl_2$ both at 20°C, which served as a comparison to investigate any influence from the addition of $CaCl_2$.

Waters per Tail/Head - Used to represent a hydration parameter, indicates the number of water molecules associated with each lipid head and tail in the bilayer. It is derived by back calculating the number of water molecules required to achieve the required change in scattering length from that of a pure lipid layer.

Area per Molecule (APM) - A parameter which offers a direct representation of the lipid spacing within the bilayer. It is calculated from the thickness of both the lipid and tail layers:

$$\text{Head Thickness} = \frac{\text{Molecular Volume}_{Head} + (30\text{Å} \times \text{Waters per Head})}{\text{APM}}$$

$$\text{Tail Thickness} = \frac{\text{Molecular Volume}_{Tail} + (30\text{Å} \times \text{Waters per Tail})}{\text{APM}}$$

Here the head and tail thickness parameters are linked with the scattering lengths and hydrations for each component.

Global/Local Roughness – Global roughness is linked across all layers to represent the overall fluctuations in the membrane and the local roughness for each head and tail group.

Table 5: Best fit parameters for al-PC SAM alone and with 10mM $CaCl_2$ at 20°C

Layer	Thickness/Å		Roughness/Å		Hydration/%	
	0mM	10mM	0	10mM	0	10mM
Silicon dioxide	14.5 ± 0.7	14.5 ± 0.7	4	4	32.2 ± 3.7	32.2 ± 3.7
SAM	19.3 ± 6.4	15.8 ± 5.1	9.8 ± 2.9	14.0 ± 0.6	10 ± 0.5	10.0 ± 1.9
al - PC Tails	12.0 ± 1.4	12.0 ± 3.3	6.8 ± 2.0	9.7 ± 1.5	42.6 ± 12.9	25.2 ± 11.1
al -PC Heads	9	9			65.1 ± 6.1	55.5 ± 2.6

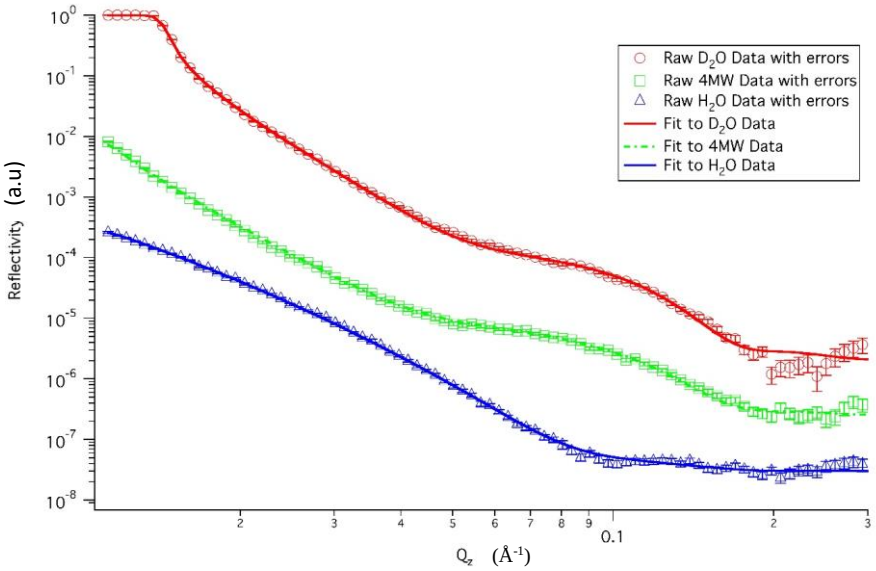

Figure 17a: Neutron reflectivity data for al-PC SAM alone.

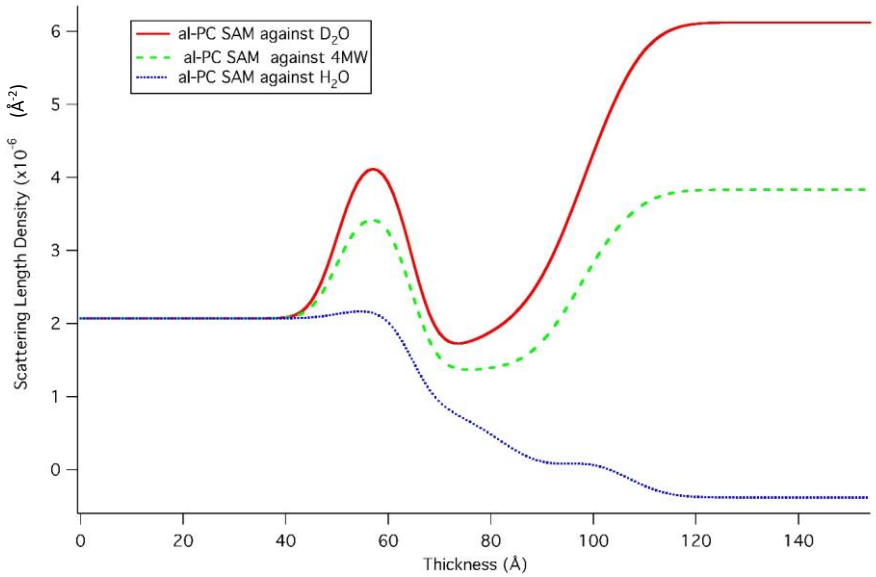

Figure 17b: SLD profile for al – PC SAM alone.

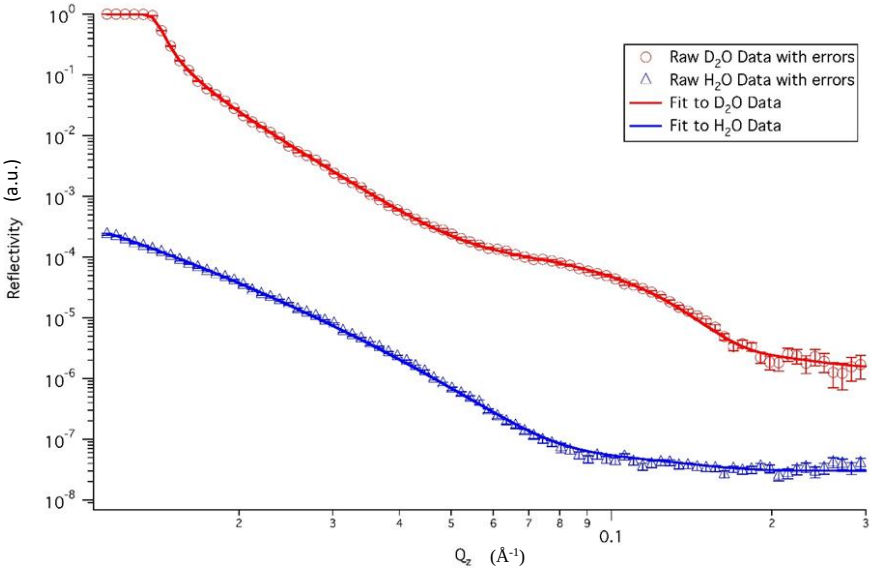

Figure 18a: Reflectivity Data for an al-PC SAM with 20 mM $CaCl_2$ at 20°C.

Commented [H1]: Please correct into subscript

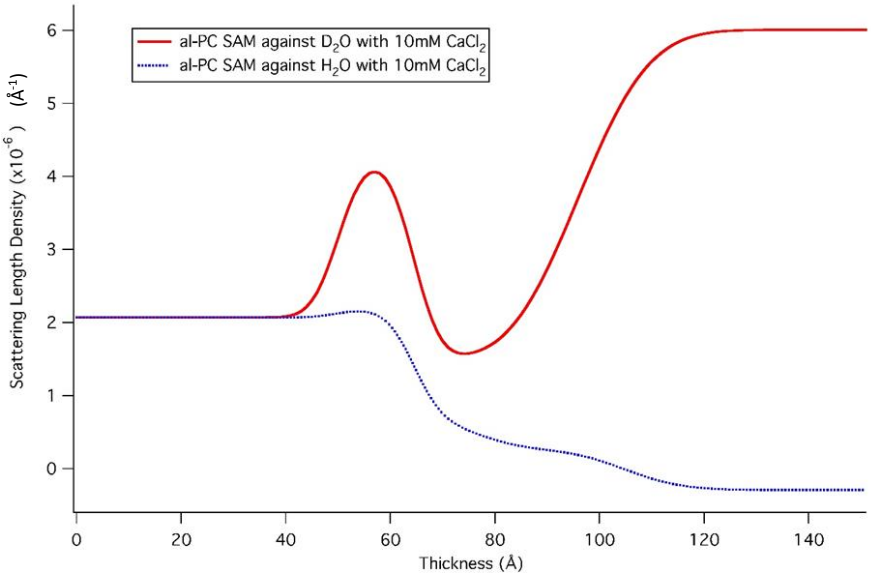

Figure 18b: SLD for an al-PC SAM with 20mM $CaCl_2$ at 20°C.

From the values displayed in Table 5 it is apparent that there is little change experienced by the layer with the addition of 10mM of $CaCl_2$. The first noticeable difference is the decrease in thickness for the SAM. This correlates to previous literature which described how an increase in Ca ion results in increased headgroup packing in monolayers[94]. This may have not occurred with the al-PC heads as they have a higher degree of freedom than those of the SAM. The loss of hydration experienced by the al-PC layer is most likely due to the calcium ions penetrating the layer and displacing the hydration water. The binding of Ca^{2+} also changes the tilt angle of the phosphate head groups[92], which further impacts the mobility of the tails as they are constricted. This increased disorder would lead to increased roughness.

ii) Gel Phase Interaction – $CaCl_2$ at 20°C

A floating bilayer was deposited onto a al-PC SAM functionalised substrate. This was kept at 20°C using a controlled water bath. Different concentrations of $CaCl_2$ ranging from 1 -1000mM were pumped through from stock solutions. The reflectivity data was also fitted using Rascal. The reflectivity data and SLD profiles for the bilayer alone and under the various $CaCl_2$ concentrations are presented below in figures 19 and 20. It is evident that a bilayer was successfully deposited[95], which is later confirmed from the values obtained from the neutron data, more specifically the bilayer area per molecule.

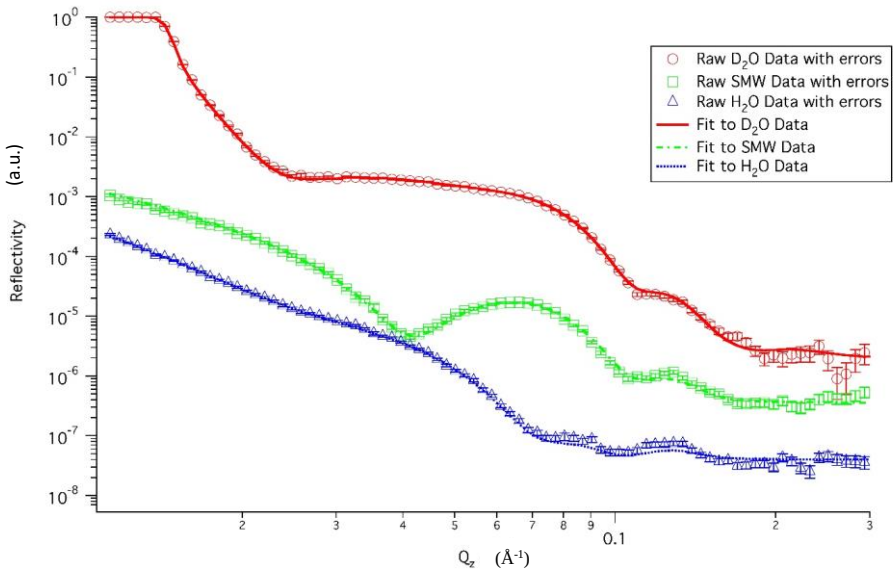

Figure 19a: Neutron reflectivity data for the hDPPC bilayer alone at 20°C on a al-PC SAM.

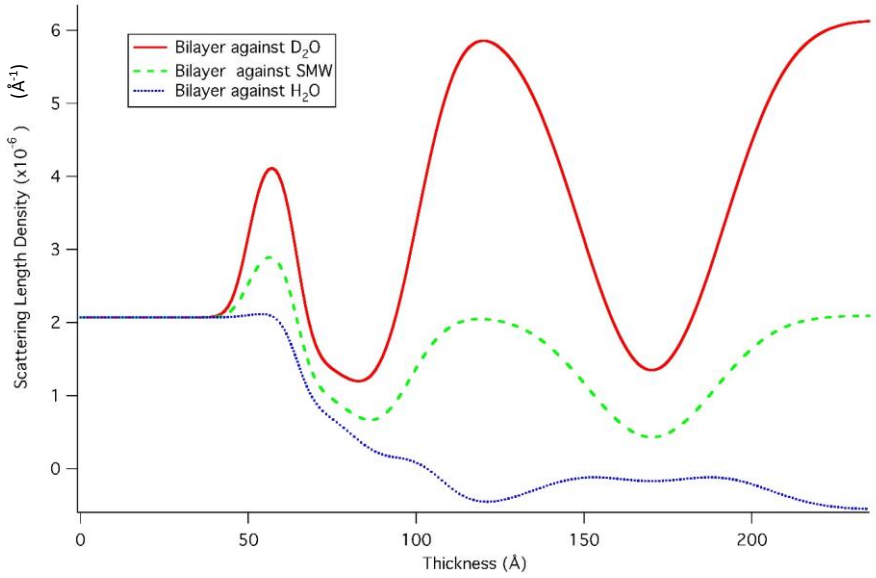

Figure 19b: SLD profile for the hDPPC bilayer alone at 20°C on a al-PC SAM

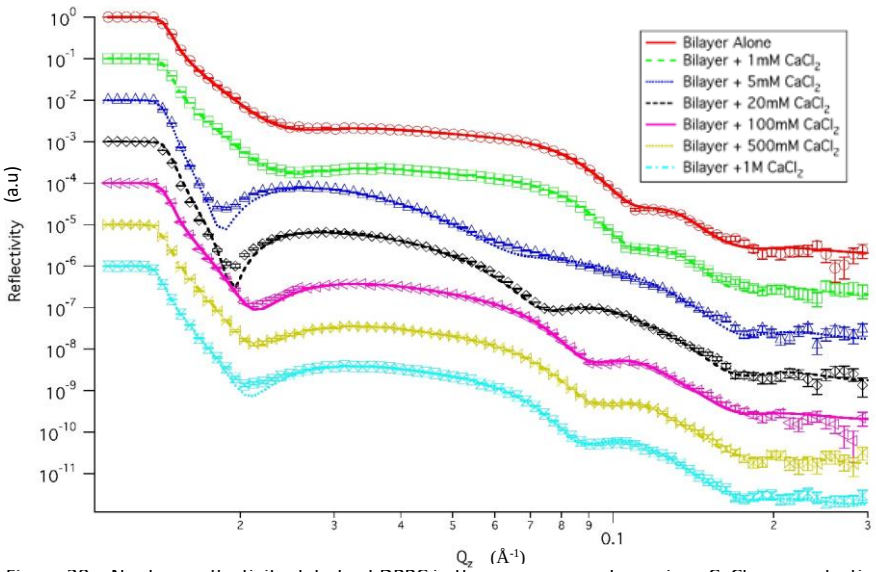

Figure 20a: Neutron reflectivity data for hDPPC in the gel phase under various $CaCl_2$ concentrations

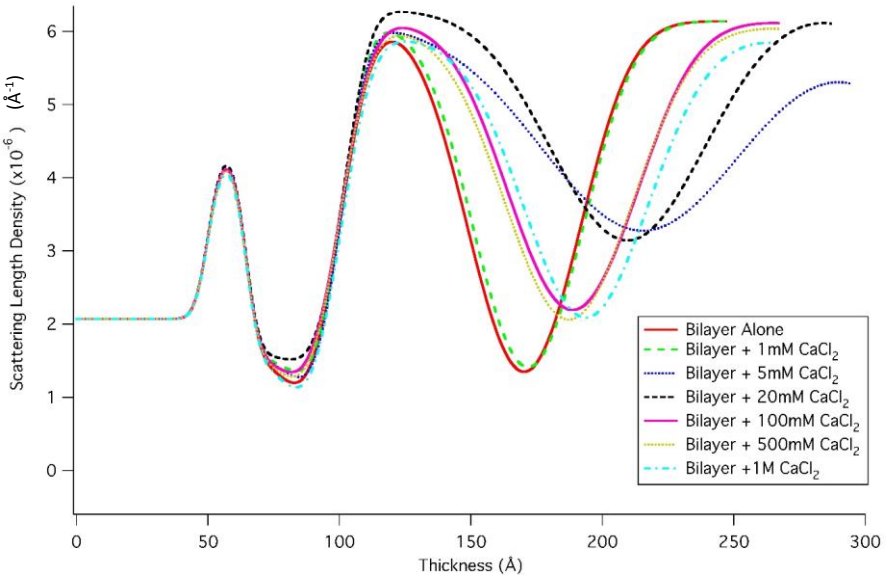

Figure 20b: SLD profile for hDPPC in the gel phase under various $CaCl_2$ concentrations.

Table 6: Values for parameters measured from neutron reflectivity for hDPPC in the gel phase under various $CaCl_2$ concentrations

				Water Molecules per Lipid		**Roughness/ Å**	
	CW Thickness/Å	**Al-PC Filling In**	**Bilayer APM/ Å² molecule⁻¹**	**Head**	**Tail**	**Global**	**Local**
Bilayer alone	38.3 ± 2.4	31.9 ± 3.8	59.5 ± 1	9.4 ± 5.9	3.1 ± 2.1	14 ± 0.5	5 ± 0.9
1mM $CaCl_2$	38.7 ± 3.5		61.1 ± 0.8	11.3 ± 5.8	3.5 ± 2.7	13.8 ± 1.1	4.6 ± 2.1
5mM $CaCl_2$	81.0 ± 7.5	27.2 ± 4.3	53.2 ± 2.8	9.9 ± 6.4	0 ± 0.6	34.7 ± 3.6	8.3 ± 6.3
20mM $CaCl_2$	76.3 ± 8.1		65.9 ± 4.4	6.1 ± 1.6	13.5 ± 5.2	23.7 ± 2.8	4.5 ± 2.8
100mM $CaCl_2$	55.5 ± 2.0		62.8 ± 1.3	8.4 ± 3.6	9.7 ± 0.8	17.5 ± 0.2	2.2 ± 3.9
500mM $CaCl_2$	51.6 ± 1.4		60.3 ± 2.1	15.1 ± 2.2	5.8 ± 3.6	18.3 ± 4.4	2.0 ± 0.8
1M $CaCl_2$	67.6 ± 1.7		62.5 ± 1.4	3.0 ± 0.6	0.0 ± 0.4	20.5 ± 1.9	0.6 ± 1.1

Table 6 above contains the values for the parameters measured from the neutron reflectivity data. Here we can see how the floating bilayer can fill in the Al-PC layer by infiltrating the gaps. However, as the concentration of $CaCl_2$ increases to 5mM there is a slight decrease in Al-PC filling but a large increase in central water thickness. This may suggest that the bilayer 'filling in' the Al-PC layer is somewhat made obsolete by the possible Ca ion bridging. Ca bridging in both the Al-PC layer and the floating bilayer would mean less water is able to penetrate the layers and is therefore subject to repulsion which would explain the increase in the central water thickness. Although when the concentration is increased from 5 to 20 mM there is a slight decrease in the central water thickness but there was also the largest occurring increase in water molecules per lipid tail. Similar to the QCM and Isotherm data this significant change between these two concentrations implies an important change occurring with the ion – lipid interaction. The QCM data suggested Ca Ion saturation of sorts which would result in ion repulsion and would further lead to displacement in the bilayer allowing water molecules to penetrate deeper. Looking at the global and local roughness further implies this as the values from 1 to 5 to 20mM follows the same pattern. From 1mM to 5 mM there is a larger increase in global roughness. Along with the increase in central water thickness, it is likely that at this point the bilayer is unstable due to the $CaCl_2$ increase, which may be due to an uneven distribution of Ca ion bridging. From 5 to 20mM this appears to decrease along with the water thickness, which likely due to an equilibrium being met where there is an even amount of bridging which stabilises the bilayer hence the decrease in global and local roughness (figure 21).

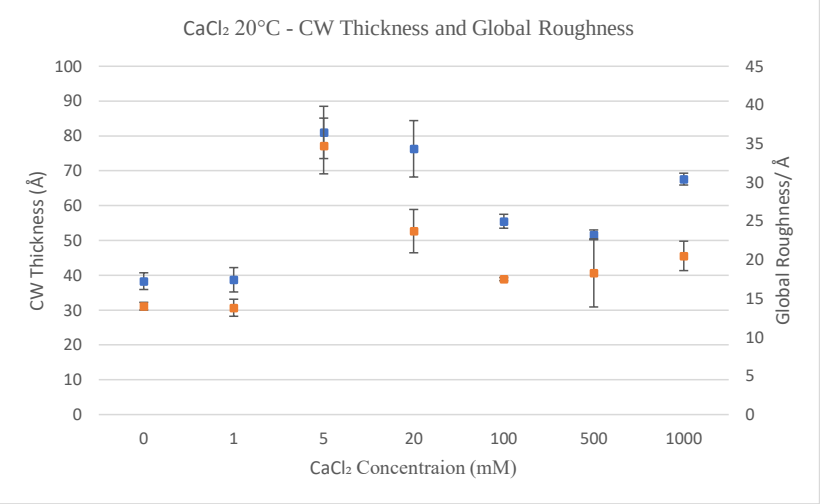

Figure 21: Central water thickness and Global Roughness with varying $CaCl_2$ concentrations at 20°C

When looking at the water molecules per head, there is an expected initial increase due to the hydrophilic nature of the lipid heads. Then a slight decrease from 1 to 5 mM, which is expected due to the displacement of water molecules by Ca ions. Here there is also a decrease in the bilayer APM; this trend has been reported in previous literature when looking at the lipid area compression due to Ca ion interactions with DMPC lipid bilayers[96]. Although the direct cause of reduction in APM is slightly unclear and could be a result of the magnitude of the repulsive forces, an increase of the

attractive forces, or a combination of both. The water molecules per head decreases from 5 to 20mM whilst the water molecules per lipid tails increases. This is also accompanied by an increase in APM, which suggests that Ca ions are increasingly displacing any water molecules associated with the phosphate head group but not those within the lipid tails. The increase in water molecules per lipid tail relates to the decrease in local roughness as the increased amount of water in between the lipid tails would increase the rigidity and therefore the stability of the bilayer. From 20 – 500mM the water molecules per head begins to increase whilst the opposite occurs for the lipid tails. This is likely due to the electrostatic repulsion and the improved lipid packing, which also led to a decrease in local roughness. At 1M there is a significant drop in water molecules per head and a less decreases in tail hydration. It appears that at higher concentrations the membrane becomes dehydrated, leading to an increase in the central water thickness which occurred as a result of an increased bilayer separation from the Al-PC layer. This is due to an less Van de Waals interaction which positively correlates to increasing Ca^{2+} concentrations[97].

iii) Fluid Phase interaction - $CaCl_2$ at 50°C

A hDPPC floating bilayer was deposited onto an al-PC SAM as per prior method for the gel phase interaction, however the bilayer was heated to 50°C instead. Again, various concentrations of $CaCl_2$, this time ranging from 1-100mM, were pumped through from stock solutions. Reflectivity data was fitted using Rascal, see figure 22. The values for the al-PC and SAM are displayed below in Table 7. A different SAM and different substrate were used, and these were characterized as a batch. From the values it is evident that the SAM was successfully deposited, and the al-PC tethered to the SAM.

Table 7: Best fit parameters for Al -PC SAM with errors for the Fluid Phase interaction

Layer	Thickness/Å	Roughness/Å	Hydration/%
Silicon dioxide	15.3	4.0	24.5
SAM	11.9	4.0	20.1
al - PC Tails	17.0 ± 0.8		
al -PC Heads	9.0	6.5 ± 0.5	26.3 ± 1.9

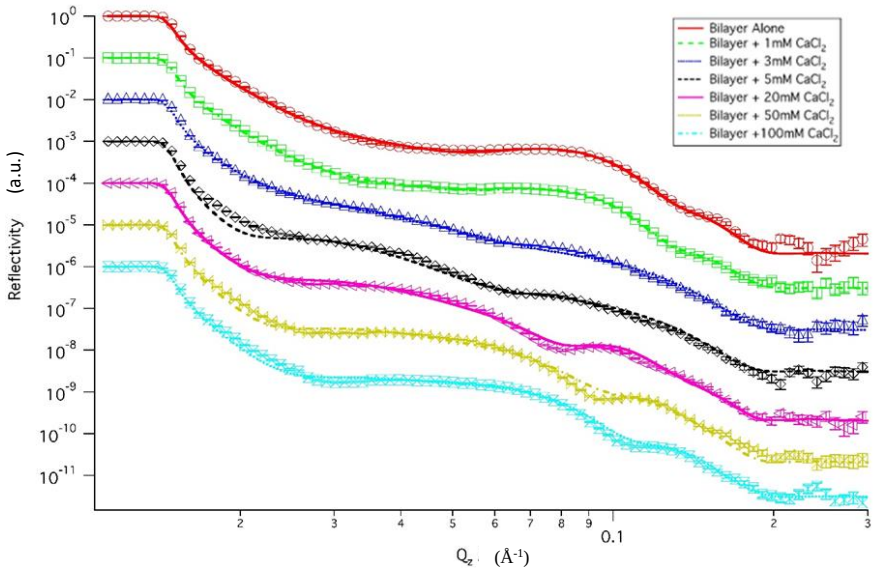

Figure 22a: Neutron Reflectivity data for hDPPC in the Fluid Phase under various $CaCl_2$ concentrations

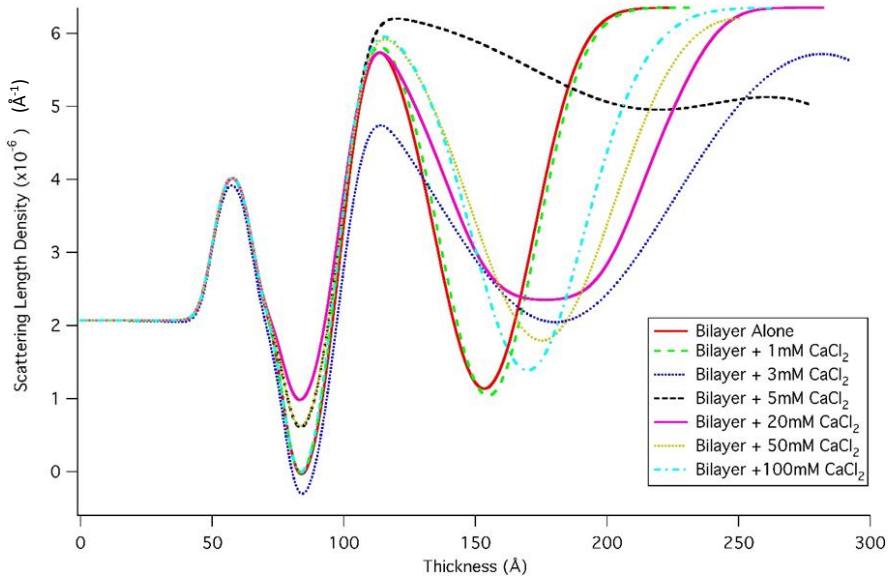

Figure 22b: SLD profile for hDPPC in the Fluid Phase under various $CaCl_2$ concentrations.

Table 8: Values for parameters measured from Neutron Reflectivity for hDPPC in the Fluid Phase under various $CaCl_2$ concentrations.

			Bilayer APM/ Å² molecule⁻¹	Water Molecules per Lipid		Roughness/ Å	
	CW Thickness/Å	al-PC Filling In		Head	Tail	Global	Local
Bilayer Alone	22.2 ± 3.4		62.3 ± 2.2	18.0 ± 4.4	0 ± 0.5	12.1 ± 4.7	2.6 ± 1.7
1mM $CaCl_2$	23.8 ± 5.3		62.8 ± 1.3	17.1 ± 9.7	0 ± 0.1	12.4 ± 2.1	3.7 ± 3.6
3mM $CaCl_2$	14.7 ± 4.4	26.3 ± 6.2	31.0 ± 5.5	20.5 ± 1.9	2.7 ± 3.8	35.0 ± 6.9	6.9 ± 5.2
5mM $CaCl_2$	99.0 ± 6.1		70.0 ± 0.7	3.0 ± 0.1	0 ± 0.2	43.5 ± 9.9	6.1 ± 4.7
20mM $CaCl_2$	17.4 ± 3.9		44.2 ± 1.4	21.2 ± 2.5	19.8 ± 2.4	8.9 ± 5.6	8.1 ± 4.9
50mM $CaCl_2$	45.2 ± 4.4	16.1 ± 2.1	49.9 ± 1.1	3.2 ± 2.8	0.1 ± 2	22 ± 1.8	3.4 ± 4.9
100mM $CaCl_2$	24.3 ± 1.8	26.3 ± 4.7	53.8 ± 3.0	34.7 ± 3.2	0 ± 1.5	14.6 ± 2.3	7.3 ± 4.1

Table 8 above contains the values for the measured parameters from the neutron reflectivity data for hDPPC under $CaCl_2$ at 50°C. Here it is evident that there is still some filling in occurring within the al- PC layer but slightly less than that which occurred for the gel phase. The area per molecule values tend to fluctuate more for the fluid phase with the highest being measured as 70 APM and the lowest at 31 APM, which is marginally different to the range of 65.9 -53 APM for the gel phase. When looking at the central water thickness there is a similar trend occurring around 5mM. From 1-5 mM there is a large increase, then a drop from 5- 20mM, for the fluid phase the values of the differences here are much more significant. When comparing the values of the waters per head/tail, the waters per head for 50°C are almost double of that in the gel phase, however the waters per tails remain low and more similar to those at 20°C. Yet there is still that large increase in waters per tail from 5 to 20mM. Interestingly though, this drops from 19.8 to 0.1 from 20 to 50 mM. Overall, the values for the roughness tend to be lower for the fluid phase than the gel phase, however there is that large increase in global roughness from 1 to 5 mM where the values nearly triple. This then decreases afterwards which occurs for both phases. This change in roughness (See figure 23) is most likely a result of conformational changes within the bilayer due to calcium binding.

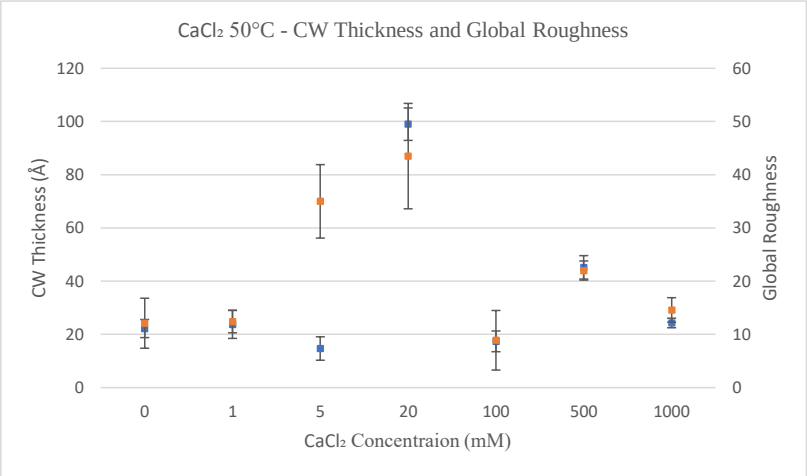

Figure 23: Central water thickness and Global Roughness with varying $CaCl_2$ concentrations at 50°C

When the Ca ions bind to the phosphate group its dipole orientation changes from the tangential to the normal direction with the $–N^+(CH_3)_3$ group outward from the bilayer surface. This would also account for the swelling within the bilayer. The Ca^{2+}- DPPC complex causes a positive net charge which produces an electric field in both the plane and perpendicular direction to the bilayer, because of this the zwitterions of the DPPC molecules are orientated towards the bound calcium ions. As a result, the long-range attraction between the bound Ca^{2+} and the DPPC molecules produces a large lateral pressure in the hydrophobic part of the bilayer, therefore as the concentration of calcium increases the distance between the Ca^{2+} ion decreases[98,99]. This effect on lipid packing would also explain the decrease in the bilayer area per molecule from 1 -5 mM.

7) Conclusion

a) QCM

Using QCM experiments provided evidence of the mass loss caused by the addition of both sodium chloride and calcium chloride. Interestingly this remains in contradiction with previous research[17] that suggested that some ion-lipid bonding occurred although limited, which would result in a mass gain. However, many of these studies were difficult to translate or compare to QCM work practically since many are computational based and rely on QCM-D[100]. Overall $CaCl_2$ appeared to have a greater impact on the bilayer than NaCl, which is indicated as the addition of $CaCl_2$, 0-20 mM resulted in the largest mass loss over the NaCl runs. Prior research has demonstrated how calcium ions have a greater interaction with the DPPC bilayers over sodium ions[101], penetrating deeper and coordinating to the phosphate oxygens much more than Na^+ ions. Contrarily, with the QCM, the addition of $CaCl_2$ resulted in the largest mass loss, the biggest mass losses occurred for both salts after 5mM which may relate to other significant results that were obtained between 5-20mM for the isotherms and neutron reflectometry experiments. Unfortunately the QCM data alone is unable to provide insight into the mechanism behind the mass loss but it does give reason for further investigation. Due to some erratic trend illustrated in the NaCl runs and the fault in the QCM system, it is imperative that this work is repeated for many more runs in order to obtain a more sophisticated and reliable comparison.

b) Langmuir isotherms:

The isotherms were conducted much more successfully and provided a more in-depth review of the salt interactions. The isotherms focused on the hDPPC monolayer with the addition of NaCl and $CaCl_2$. Like the result obtained with the QCM, those obtained from the Langmuir isotherms display how the addition of $CaCl_2$ has the more significant impact on DPPC, however this was concerning monolayers. At 'lift off' or low surface pressures 0-10 m/Nm, the addition of NaCl and $CaCl_2$ both resulted in a decrease in area per molecule, although the magnitude was less for NaCl. Like the QCM data, significant trends started to appear around 5mM. When comparing the $CaCl_2$ and NaCl isotherms at 5-20 mM, 5 overlaps 20 mM for $CaCl_2$ but not for NaCl, which was somewhat expected from prior literature[79], however the fact that it occurs at 5 mM further indicates the significance of this concentration and its effect on the DPPC membranes. The difference between 5 and 20 mM on both isotherms remained the greatest and implied disruption of the lipid, which could be related to mass loss and therefore could correlate with the results from the QCM experiments. At higher concentrations of both salts, moving towards the condensed phase, the isotherms appear similar which would signify how the monolayer is behaving the same regardless of the salt influence at that stage.

c) Neutron Reflectometry

Neutron reflectometry data was obtained for a single bilayer under $CaCl_2$ concentrations 1mM -1M. The single bilayer data failed to reveal much in depth information about the salt influence as the resolution was too high, that being said the overlap of the scattering curves express how there was little to no interaction experienced between the salts and bilayer. This alone may not have provided sufficient insight, therefore further neutron experiments were conducted, this time using a model of a self-assembled monolayer 'SAM', and a tethered al -PC layer, with a floating bilayer. This model considered more specific parameters such as 'waters per head/tail' and global/local roughness. These extra parameters were able to provide a more in-depth look at the movement and positioning of the individual DPPC molecules as well as the overall fluctuations of the bilayer. For the Gel phase interaction, $CaCl_2$ at 20°C, there is again significant change occurring from 5-20 mM, a large increase in central water thickness to 5mM. This suggested Ca ion bridging, however the decrease in CW thickness from 5-20mM accompanied with an increase in water molecules per lipid tail further indicated a moment where the concentration of $CaCl_2$ was optimal for the bilayer and an increase in concentration causes the bilayer to become unstable, much like that illustrated in the isotherms with the monolayer collapse. For the fluid phase, $CaCl_2$ at 50°C, there were similar occurrences to that of the gel phase from 5-20mM, this being the trend in central water thickness and the roughness, both salts see a decrease at higher concentrations for roughness, the fact that both salts induce this further implement the theory that these particular concentrations of salt (5-20mM) have important influence on the membrane and therefore more in-depth investigations should be carried out.

8) Overall conclusion

The aim of this study was to further investigate salt interactions with lipid membranes, more specifically sodium chloride and calcium chloride interactions with the zwitterionic membrane hDPPC. This membrane and salts were chosen in order to closely mimic physiological conditions. A variety of techniques were implemented to further elaborate on the presence of any interactions. The QCM provided evidence of and overall mass loss with the attempt of salt deposits on the membrane bilayer which contradicted previous research, however some changes in mass implied a possible saturation around 5mM. Although due to the QCM's unreliability this would need further investigations. Isotherms were obtained which provided data on the salt interactions with monolayer leaflets of hDPPC, interestingly overlaps in the data also implied a disruption in the bilayer which may relate to the occurrence in the QCM data as they both occurred around 5-20mM. Finally, neutron reflectometry experiments were conducted with the intention of providing a more in depth look at the membrane – salt interaction, however the resolution was too high, although the overlaps in the data suggested that little interaction occurred. Besides the QCM reliability and neutron experiment resolution presenting an issue, the overall experiment did succeed in meeting the aims presented in the scope of the study, which was to provide evidence of zwitterionic membrane interactions with salts through physical experiments rather than simulations. With the evidence provided in studies such as this it can be suggested that experiments such as those conducted here combined with simulations may provide an even more coherent explanation into membrane interactions in future work.

9) Future Work

This work alone provides evidence for a potential more expanded investigation into salt interactions at around 5-20mM. However, this should be approached coherently and should consider both bilayer and monolayer studies in order to explore the nature of the calcium binding and it's effect of lipid swelling and fluctuation. Currently this most commonly conducted through simulations still[94]. Therefore, to truly expand the understanding of the mechanism behind the behaviour of the interactions, multiple techniques, including theoretical techniques should be utilized. This combination of techniques has been recently applied when studying the effect physiological macromolecules have on DPPC[102]. Using multiple techniques also provides a reliable foundation for hypothesis. This can be seen in the work conducted in this thesis, where various techniques revealed an occurring trend at certain concentrations, therefore warranting further exploration. This being said, if a QCM based study was to be conducted, QCM -D should be utilized as the dissipation provides information on viscoelasticity which has proved valuable in previous work[103]. This work and many priors have expressed how NaCl has less interaction with DPPC than $CaCl_2$, consequently it may be though as to disregard NaCl for a more extensive study however, although not essential, including NaCl provides a good comparison to determine the significance of interactions of other salts both quantitively and interpretively.

10) References

1 I. James L. Lewis, Overview of Sodium's Role in the Body, https://www.msdmanuals.com/en-gb/home/hormonal-and-metabolic-disorders/electrolyte-balance/overview-of-sodiums-role-in-the-body.

2 W. S. W. W.E.Farquhar, D.G.Edwards, C.T.Jurkovitz, *J. Am. Coll. Cardiol.*, 2015, **32**, 34–38.

3 W. J. Brown, F. K. Brown and I. Krishan, *Circulation*, 1971, **43**, 508–519.

4 I. Y. Kuo and B. E. Ehrlich, *Cold Spring Harb. Perspect. Biol.*, 2015, **7**, 1–14.

5 E. Stubblefield and G. C. Mueller, *Cancer Res.*, 1960, **20**, 1646–1655.

6 D. C. Fish, J. P. Dobbs and A. D. J. M. Elliott, *In Vitro*, 1973, **9**, 10–15.

7 E. V. A. Kurth, G. R. Cramer, A. Lauchli and E. Epstein, *Cell*, 1986, 1102–1106.

8 K. F. Zhao, J. Song, H. Fan, S. Zhou and M. Zhao, *J. Integr. Plant Biol.*, 2010, **52**, 468–475.

9 Y. I. T.Udou, *J. Genral Microbiol.*, 2016, 69–74.

10 A. K. Bandyopadhyay and H. M. Sonawat, *Biophys. J.*, 2000, **79**, 501–510.

11 Y. -C Shih, J. M. Prausnitz and H. W. Blanch, *Biotechnol. Bioeng.*, 1992, **40**, 1155–1164.

12 A. C. Dumetz, A. M. Snellinger-O'Brien, E. W. Kaler and A. M. Lenhoff, *Protein Sci.*, 2007, **16**, 1867–1877.

13 S. McLaughlin, N. Mulrine, T. Gresalfi, G. Vaio and A. McLaughlin, *J. Gen. Physiol.*, 1981, **77**, 445–473.

14 R. J. Alsop, R. Maria Schober and M. C. Rheinstädter, *Soft Matter*, 2016, **12**, 6737–6748.

15 H. I. Petrache, S. Tristram-nagle, D. Harries, N. Ku, F. John and V. A. Parsegian, *Jounral Lipid Res.*, 2009, **47**, 302–309.

16 P. Jurkiewicz, L. Cwiklik, A. Vojtíšková, P. Jungwirth and M. Hof, *Biochim. Biophys. Acta - Biomembr.*, 2012, **1818**, 609–616.

17 S. A. Pandit, D. Bostick and M. L. Berkowitz, *Biophys. J.*, 2003, **85**, 3120–3131.

18 H. H. G. Tsai, W. X. Lai, H. Da Lin, J. Bin Lee, W. F. Juang and W. H. Tseng, *Biochim. Biophys. Acta - Biomembr.*, 2012, **1818**, 2742–2755.

19 A. M. Nesterenko and Y. A. Ermakov, *Biochem. Suppl. Ser. A Membr. Cell Biol.*, 2012, **6**, 320–328.

20 C. T. M. Le, A. Houri, N. Balage, B. J. Smith and A. Mechler, *Mol. Pharm.*, 2019, **5**, 1–9.

21 S. Freeman, M. Harrington and J. Sharp, *Biol. Sci.*, 2011, **6**, 99–124.

22 T. Kotnik, P. Kramar, G. Pucihar, D. Miklavčič and M. Tarek, *IEEE Electr. Insul. Mag.*, 2012, **28**, 14–23.

23 T. Y. Tsong, *Biophys. J.*, 1991, 297–306.

24 K. A. Riske and R. Dimova, *Biophys. J.*, 2006, **91**, 1778–1786.

25 E. Gongadze, S. Petersen, U. Beck and U. van Rienen, *Comsol Conf.*

26 Malvern, *Zetasizer Nano Serles Tech. Note. MRK654-01*, 2000, **2**, 1–6.

27 A. Melcrová, S. Pokorna, S. Pullanchery, M. Kohagen, P. Jurkiewicz, M. Hof, P. Jungwirth, P. S. Cremer and L. Cwiklik, *Sci. Rep.*, 2016, **6**, 1–12.

28 J. A. Cohen and M. Cohen, *Biophys. J.*, 1981, **36**, 623–651.

29 S. G. A. McLaughlin, G. Szabo and G. Eisenman, *J. Gen. Physiol.*, 1971, **58**, 667–687.

30 H. Jing and S. Das, *Electrophoresis*, 2018, **39**, 752–759.

31 S. J. Mattingly, M. G. Otoole, K. T. James, G. J. Clark and M. H. Nantz, *Langmuir*, 2015, **31**, 3326–3332.

32 S. A. Pandit, D. Bostick and M. L. Berkowitz, *Biophys. J.*, 2003, **84**, 3743–3750.

33 P. Jurkiewicz, L. Cwiklik, A. Vojtíšková, P. Jungwirth and M. Hof, *Biochim. Biophys. Acta - Biomembr.*, 2012, **1818**, 609–616.

34 V. Knecht and B. Klasczyk, *Biophys. J.*, 2013, **104**, 818–824.

35 D. Harries, S. May and A. Ben-Shaul, *Soft Matter*, 2013, **9**, 9268–9284.

36 A. A. Gurtovenko and I. Vattulainen, *J. Phys. Chem. B*, 2008, **112**, 1953–1962.

37 F. M. Goñi, *Biochim. Biophys. Acta - Biomembr.*, 2014, **1838**, 1467–1476.

38 S. J. Singer and G. L. Nicolson, *Science (80-.).*, 1972, **175**, 720–731.

39 J. F. Nagle, H. I. Petrache, N. Gouliaev, S. Tristram-Nagle, Y. Liu, R. M. Suter and K. Gawrisch, *Phys. Rev. E - Stat. Physics, Plasmas, Fluids, Relat. Interdiscip. Top.*, 1998, **58**, 7769–7776.

40 G. Fragneto, T. Charitat, E. Bellet-Amalric, R. Cubitt and F. Graner, *Langmuir*, 2003, **19**, 7695–7702.

41 W. Helfrich, *Zeitschrift fur Naturforsch. - Sect. A J. Phys. Sci.*, 1978, **33**, 305–315.

42 J. F. Nagle and S. Tristram-Nagle, *Biochim. Biophys. Acta - Rev. Biomembr.*, 2000, **1469**, 159–195.

43 T. J. Mcintosh, N. Carolina and S. A. Simqn, 1994, 27–51.

44 J. C. Shillcock and U. Seifert, *Biophys. J.*, 1998, **74**, 1754–1766.

45 J. H. Ipsen, K. Jørgensen and O. G. Mouritsen, *Biophys. J.*, 1990, **58**, 1099–1107.

46 E. Falck, T. Róg, M. Karttunen and I. Vattulainen, *J. Am. Chem. Soc.*, 2008, **130**, 44–45.

47 N. Watanabe, K. Suga and H. Umakoshi, *J. Chem.*, , DOI:10.1155/2019/4867327.

48 M. Pasenkiewicz-Gierula, K. Baczynski, M. Markiewicz and K. Murzyn, *Biochim. Biophys. Acta - Biomembr.*, 2016, **1858**, 2305–2321.

49 T. Shimanouchi, M. Sasaki, A. Hiroiwa, N. Yoshimoto, K. Miyagawa, H. Umakoshi and R. Kuboi, *Colloids Surfaces B Biointerfaces*, 2011, **88**, 221–230.

50 D. P. Tieleman, S. J. Marrink and H. J. C. Berendsen, *Biochim. Biophys. Acta - Rev. Biomembr.*, 1997, **1331**, 235–270.

51 K. V. Damodaran, K. M. Merz and B. P. Gaber, *Biochemistry*, 1992, **31**, 7656–7664.

52 R. L. Baldwin, *Biophys. J.*, 1996, **71**, 2056–2063.

53 X. Tadeo, B. López-Méndez, D. Castaño, T. Trigueros and O. Millet, *Biophys. J.*, 2009, **97**, 2595–2603.

54 A. Aroti, E. Leontidis, M. Dubois and T. Zemby, *Biophys. J.*, 2007, **93**, 1580–1590.

55 J. Kherb, S. C. Flores and P. S. Cremer, *J. Phys. Chem. B*, 2012, **116**, 7389–7397.

56 H. Maity, A. N. Muttathukattil and G. Reddy, *J. Phys. Chem. Lett.*, 2018, **9**, 5063–5070.

57 J. M. Peula-García, J. L. Ortega-Vinuesa and D. Bastos-González, *J. Phys. Chem. C*, 2010, **114**, 11133–11139.

58 M. W. W. K.D. Collins, *Q. Rev. Biophys.*, 1985, **18**, 323–422.

59 Y. Marcus, *Pure Appl. Chem.*, 2010, **82**, 1889–1899.

60 Y. Zhang and P. S. Cremer, *Curr. Opin. Chem. Biol.*, 2006, **10**, 658–663.

61 M. Boström, D. R. M. Williams and B. W. Ninham, *J. Phys. Chem. B*, 2002, **106**, 7908–7912.

62 W. Helfrich, *Zeitschrift fur Naturforsch. - Sect. C J. Biosci.*, 1973, **28**, 693–703.

63 J. S. Hub, T. Salditt, M. C. Rheinstädter and B. L. De Groot, *Biophys. J.*, 2007, **93**, 3156–3168.

64 X.-M. Yu, B. R. Groveman, X.-Q. Fang and S.-X. Lin, *Health (Irvine. Calif).*, 2010, **02**, 8–15.

65 G. H. R. Bagur, *Mol. Cell*, 2017, **6**, 780–788.

66 P. R. Ashcroft, Frances M, *Nat. Rev. Endocrinol.*, 2013, **9**, 660–669.

67 R. A. Dluhy, D. G. Cameron, H. H. Mantsch and R. Mendelsohn, *Biochemistry*, 1983, **22**, 6318–6325.

68 U. R. Pedersen, C. Leidy, P. Westh and G. H. Peters, *Biochim. Biophys. Acta - Biomembr.*, 2006, **1758**, 573–582.

69 M. Roux and M. Bloom, *Biochemistry*, 1990, **29**, 7077–7089.

70 A. Melcrová, S. Pokorna, M. Vošahlíková, J. Sýkora, P. Svoboda, M. Hof, L. Cwiklik and P. Jurkiewicz, *Langmuir*, 2019, **35**, 11358–11368.

71 M. Javanainen, A. Melcrová, A. Magarkar, P. Jurkiewicz, M. Hof, P. Jungwirth and H. Martinez-Seara, *Chem. Commun.*, 2017, **53**, 5380–5383.

72 A. Magarkar, V. Dhawan, P. Kallinteri, T. Viitala, M. Elmowafy, T. Róg and A. Bunker, *Sci. Rep.*, 2014, **4**, 1–5.

73 R. D. Porasso and J. J. López Cascales, *Colloids Surfaces B Biointerfaces*, 2009, **73**, 42–50.

74 Y. N. Kaznessis, S. Kim and R. G. Larson, *Biophys. J.*, 2002, **82**, 1731–1742.

75 W. Zhao, T. Róg, A. A. Gurtovenko, I. Vattulainen and M. Karttunen, *Biophys. J.*, 2007, **92**, 1114–1124.

76 D. A. Doshi, A. M. Dattelbaum, E. B. Watkins, C. J. Brinker, B. I. Swanson, A. P. Shreve, A. N. Parikh and J. Majewski, *Langmuir*, 2005, **21**, 2865–2870.

77 B. W. Koenig, S. Krueger, W. J. Orts, C. F. Majkrzak, N. F. Berk, J. V. Silverton and K. Gawrisch, *Langmuir*, 1996, **12**, 1343–1350.

78 A. Junghans, E. B. Watkins, R. D. Barker, S. Singh, M. J. Waltman, H. L. Smith, L. Pocivavsek and J. Majewski, *Biointerphases*, 2015, **10**, 019014.

79 N. Yousefi and N. Tufenkji, *Front. Chem.*, 2016, **4**, 1–8.

80 E. Hellstrand, M. Grey, M. L. Ainalem, J. Ankner, V. T. Forsyth, G. Fragneto, M. Haertlein, M. T. Dauvergne, H. Nilsson, P. Brundin, S. Linse, T. Nylander and E. Sparr, *ACS Chem. Neurosci.*, 2013, **4**, 1339–1351.

81 B. S. Barker, G. T. Young, C. H. Soubrane, G. J. Stephens, E. B. Stevens and M. K. Patel, *Ion Channels*, Elsevier Inc., 2017.

82 E. Hutchinson, *J. Chem. Educ.*, 1955, **32**, 342.

83 S. Garcia-Manyes and F. Sanz, *Biochim. Biophys. Acta - Biomembr.*, 2010, **1798**, 741–749.

84 D. B. A.S.Colburn, N.Meeks, S.T.Weinman, *Ind. Eng. Chem. Res.*, 2016, **55**, 4089–4097.

85 G. Rudolph, T. Virtanen, M. Ferrando, C. Güell, F. Lipnizki and M. Kallioinen, *J. Memb. Sci.*, 2019, **588**, 117221.

86 V. Sarapulova, E. Nevakshenova, X. Nebavskaya, A. Kozmai, D. Aleshkina, G. Pourcelly, V. Nikonenko and N. Pismenskaya, *J. Memb. Sci.*, 2018, **559**, 170–182.

87 R. M. DuChanois, R. Epsztein, J. A. Trivedi and M. Elimelech, *J. Memb. Sci.*, 2019, **581**, 413–420.

88 C. Mista, M. Zalazar, A. Pealva, M. Martina and J. M. Reta, *J. Phys. Conf. Ser.*

89 A. Ładniak, M. Jurak and A. E. Wiącek, *Adsorption*, 2019, **25**, 469–476.

90 A. M. J.C.Tejedor, A.Santamaria, D.Pereira, *Coatings*, 2020, 10, 507

91 D. F. Kienle, J. V. De Souza, E. B. Watkins and T. L. Kuhl, *Anal. Bioanal. Chem.*, 2014, **406**, 4725–4733.

92 N. N. Casillas-Ituarte, X. Chen, H. Castada and H. C. Allen, *J. Phys. Chem. B*, 2010, **114**, 9485–9495.

93 A. S. Petrov, J. Funseth-Smotzer and G. R. Pack, *Int. J. Quantum Chem.*, 2005, **102**, 645–655.

94 M. Javanainen, W. Hua, O. Tichacek, P. Delcroix, L. Cwiklik and H. C. Allen, *Langmuir*, 2020, **36**, 15258–15269.

95 R. Barker, University of Bath, 2012.

96 D. Huster, G. Paasche, U. Dietrich, O. Zschörnig, T. Gutberlet, K. Gawrisch and K. Arnold, *Biophys. J.*, 1999, **77**, 879–887.

97 G. Pabst, A. Hodzic, J. Štrancar, S. Danner, M. Rappolt and P. Laggner, *Biophys. J.*, 2007, **93**, 2688–2696.

98 M. . Aruga.S, Kataoka.R, *Biophys. Chem.*, 1985, **21**, 265–275.

99 D. Uhríková, N. Kučerka, J. Teixeira, V. Gordeliy and P. Balgavý, *Chem. Phys. Lipids*, 2008, **155**, 80–89.

100 B. Seantier and B. Kasemo, *Langmuir*, 2009, **25**, 5767–5772.

101 R. D. Porasso and J. J. López Cascales, *Colloids Surfaces B Biointerfaces*, 2009, **73**, 42–50.

102 P. Bełdowski, G. Krzysztof, Z. Dendzik, D. C. F. Wieland and R. Willumeit-römer, *Molecules*.

103 B. Scantier, C. Breffa, O. Félix and G. Decher, *J. Phys. Chem. B*, 2005, **109**, 21755–21765.